Differences in Calcium Homeostasis between Retinal Rod and Cone Photoreceptors Revealed by the Effects of Voltage on the cGMP-gated Conductance in Intact Cells

JAMES L. MILLER and JUAN I. KORENBROT

From the Department of Physiology, School of Medicine, University of California at San Francisco, San Francisco, California 94143

ABSTRACT We measured currents under voltage clamp in intact retinal rod photoreceptors with tight seal electrodes in the perforated patch mode. In the dark, membrane depolarization to voltages $\geq +20$ mV activates a time- and voltage-dependent outward current in the outer segment. This dark voltage-activated current (DVAC) increases in amplitude with a sigmoidal time course that is voltage dependent. DVAC reaches its maximum enhancement of ~30% in 4–6 s at +60 mV. DVAC is entirely suppressed by light and its current-voltage curve and reversal potential are the same as those of the photocurrent. Therefore, DVAC arises from the opening in darkness of the cGMP-gated channels of the outer segment. DVAC is blocked by BAPTA loaded into the cell's cytoplasm and is enhanced by lowering extracellular Ca^{2+} concentration. Because the cGMP-gated channels are not directly gated by voltage and because BAPTA blocks DVAC, we suggest this signal arises from a voltage-dependent decrease in cytoplasmic Ca^{2+} concentration that, in turn, activates guanylyl cyclase and causes cGMP synthesis. In rods loaded with high cytoplasmic Na^+, membrane depolarization in darkness to voltages $\geq +20$ mV inactivates the outward current in the outer segment with an exponential time course. We call this DVIC (dark, voltage-inactivated current). DVIC reflects voltage-dependent closing of the cGMP-gated channel in the dark. DVIC, too, is blocked by cytoplasmic BAPTA, and it arises from a voltage-dependent rise in cytoplasmic Ca^{2+} in darkness, which occurs only if cytoplasmic Na is high. We develop a quantitative model to calculate the rate and extent of the voltage-dependent change in cytoplasmic Ca^{2+} concentration in a normal rod. We assume that this concentration is controlled by the balance between Ca^{2+} influx through the cGMP-gated channels and its efflux through a Na^+/Ca^{2+}, K^+ exchanger. Lowered cytoplasmic Ca^{2+} is linked to guanylyl cyclase activation with characteristics determined from biochemical studies. The model considers the cytoplasmic buffering of both Ca^{2+} and cGMP. Simulated data generated by the model fit well DVAC measured in rods and also

Address correspondence to Juan I. Korenbrot, Department of Physiology, School of Medicine, Box 0444, University of California at San Francisco, San Francisco, CA 94143.

J. GEN. PHYSIOL. © The Rockefeller University Press · 0022-1295/94/11/0909/32 $2.00
Volume 104 November 1994 909–940

DVAC previously measured in cones. DVAC in cones is larger in magnitude and faster in time course than that in rods. The successful fit of DVAC by the model leads us to suggest that the activity and Ca^{2+} dependence of the enzymes of transduction are not different in rods and cones, but the quantitative features of Ca^{2+} homeostasis in the outer segment of the two receptor types differ profoundly. In general, for a given change in outer segment current, whether caused by light or by voltage, the changes in cytoplasmic Ca^{2+} are larger and faster in cones than in rods. This difference reflects specific differences between receptor types in their outer segment volume as well as in the relative fraction of the current carried by Ca^{2+} through the cGMP-gated channels, the intracellular Ca^{2+} buffering capacity and the rate of Ca^{2+} clearance from the outer segment by the Na^+/Ca^{2+}, K^+ exchanger.

INTRODUCTION

The cytoplasmic concentration of cGMP in the outer segment of rod and cone photoreceptors is relatively high in darkness and cGMP-gated ion channels are open. cGMP concentration is controlled by the continuous balance between nucleotide synthesis by guanylyl cyclase (GC) and its hydrolysis by phosphodiesterase (PDE). Brief illumination enhances the activity of PDE over that of GC, causing a decrease in cGMP and closure of the ion channels (reviewed by Pugh and Lamb, 1993; Hurley, 1992). In time, GC activity increases, PDE activity decreases, and the cGMP level returns to its starting value (reviewed by Stryer, 1991; Kaupp and Koch, 1992). The time course and light sensitivity of the cGMP changes, and thus, of the photoresponse, differ in rods and cones of the same species (Miller and Korenbrot, 1993*a*). In general, the rod photoresponse is slower and more sensitive to light than that of cones (reviewed by McNaughton, 1990; Miller, Picones, and Korenbrot, 1994). Light adaptation also differs between the receptor types. Rods adapt over a narrower range of background light intensities than do cones (reviewed by McNaughton, 1990; Miller, Picones, and Korenbrot, 1994). The mechanisms underlying these differences are unknown.

Cytoplasmic Ca^{2+} ions in the outer segment play a critical role in the modulation of the time course and sensitivity of the photoresponse. In both rods and cones, loading intracellular Ca^{2+} buffers increases the photosensitivity of the response, slows down its time course and interferes with the processes of light and dark adaptation (Korenbrot and Miller, 1986; Lamb, Matthews, and Torre, 1986; Matthews, 1991; Miller and Korenbrot, 1993*b*). Light adaptation is blocked if light-dependent changes in cytoplasmic Ca^{2+} are prevented (Fain, Lamb, Matthews, and Murphy, 1989; Matthews, Fain, Murphy, and Lamb, 1990; Nakatani and Yau, 1988). In the dark, the concentration of Ca^{2+} in the outer segment of rods and cones is maintained at a steady value by the kinetic balance between Ca^{2+} influx, via the cGMP-gated channels of the outer segment, and its efflux, via an $Na^+/Ca^{2+},K^+$ exchanger (Yau and Nakatani, 1985; Miller and Korenbrot, 1987; Lagnado, Cervetto, and McNaughton, 1992). In response to illumination, closure of the light-sensitive channels, in the presence of continuous extrusion of Ca^{2+} by the exchanger, causes a decrease in cytoplasmic Ca^{2+} concentration (Yau and Nakatani, 1985; Miller and Korenbrot, 1987). Direct measurements indicate that light flashes sufficiently bright to close all

light-sensitive ion channels cause an exponential decline in cytoplasmic Ca^{2+} (McNaughton, Cervetto, and Nunn, 1986; Ratto, Payne, Owen, and Tsien, 1988).

In the physiological concentration range (between 50 and 500 nM), Ca^{2+} modulates at least three biochemical processes in rods: (*a*) the activity of GC increases as Ca^{2+} decreases with a K_D of ~200 nM and a power dependence on Ca^{2+} concentration (Fleischman and Denisevich, 1979; Lolley and Racz, 1982; Pepe, Boero, Vergani, Panfoli, and Cugnoli, 1986; Koch and Stryer, 1988; Kawamura and Murakami, 1989). (*b*) The lifetime of light-activated PDE is prolonged as Ca^{2+} concentration decreases, a process that apparently reflects the action of Ca^{2+} on rhodopsin phosphorylation (Kawamura and Murakami, 1991; Kawamura, 1993; Lagnado and Baylor, 1994). (*c*) In the presence of added calmodulin, the Km for cGMP activation of the cGMP-gated ion channels increases as Ca^{2+} increases with a $K_{1/2}$ of ~10^{-7} M (Hsu and Molday, 1993). In these three processes the action of Ca^{2+} is not direct on the target protein (whether GC, PDE, or the channel) but is mediated by a Ca^{2+}-binding protein.

We recently reported that in single cones, membrane depolarization in the dark to voltages $\geq$ +20 mV activates the cGMP-dependent current in the outer segment (Miller and Korenbrot, 1993*b*). The activation has a sigmoidal time course and its magnitude and kinetics are voltage dependent. We called this process DVAC (dark, voltage-activated current). We suggested that DVAC arises from the activation of GC caused by a voltage-dependent decrease in cytoplasmic Ca^{2+} concentration. We tested this mechanism experimentally and we modeled it quantitatively. Model simulations matched experimental data well and the analysis of DVAC permitted us to examine the features of Ca^{2+} homeostasis and the regulation of GC activity by Ca^{2+} in cones. Our observations in cones, however, contrast those made in rods by Baylor and Nunn (1986). They found that depolarization in the dark of tiger salamander rods to $\geq$ +20 mV inactivates the cGMP-dependent current in the outer segment. The current inactivation had an exponential time course and its extent and kinetics were voltage dependent. On the other hand, Rispoli and Detwiler (1991) observed in detached rod outer segments of the gecko, DVAC-like currents in response to depolarization in the dark. These DVAC-like currents in gecko rod outer segments were slower than those we observed in intact cones.

We report here on the features of voltage-dependent currents measured in darkness in the outer segment of intact tiger salamander rods. The rods exhibit DVAC currents under normal physiological conditions, but anomalous cytoplasmic ionic composition leads to current inactivation. DVAC in rods, however, is slower in time course and smaller in extent than that in cones. Analysis of DVAC in rods with the quantitative model we first developed to explain this signal in cones suggests that the biochemical properties of the enzymes of the signal transduction cascade and their Ca^{2+} sensitivity are similar in the two receptor types. Rods and cones, on the other hand, differ profoundly in the features of their Ca^{2+} homeostasis.

MATERIALS AND METHODS

Materials

Tiger salamanders (*Ambystoma tigrinum*) in their aquatic phase were obtained from Charles Sullivan (Nashville, TN) and maintained in the laboratory at 4°C under 12 h dark-light cycles.

Concanavalin A was received from E. Y. Labs (San Mateo, CA), BAPTA and Pluronic F-127 from Molecular Probes, Inc. (Eugene, OR), Nifedipine from CalBiochem Corp. (San Diego, CA), Chelex-100 from Bio-Rad Laboratories (Richmond, CA), MEM vitamins and amino-acid supplements from the tissue culture facility at UCSF and all other chemicals from Sigma Chemical Co. (St. Louis, MO).

Retinal Dissociation, Cell Plating, and Electrical Recording

Tiger salamanders were dark adapted for 4 to 6 h and then killed and pithed in complete darkness. Under infrared illumination, aided by a video camera and monitor, eyes were hemisected and the retina isolated in standard bathing solution of composition (in millimolar): NaCl (100), KCl (2), $NaHCO_3$ (5), NaH_2PO_4 (1), $MgCl_2$ (1), $CaCl_2$ (1), glucose (10), MEM vitamins and amino acid supplements, HEPES (10), pH 7.4, osmotic pressure 232 mosM. The retina was cut and the pieces were transferred to standard solution in which glucose was isoosmotically replaced by Na-pyruvate (5 mM). The retina pieces were chopped with a razor blade in 600 μl of the pyruvate solution in a polystyrene petri dish. 250 μl of the resulting cell suspension, free of retinal fragments, were placed on a Concanavalin A-coated glass coverslip that formed the bottom of an electrophysiological recording chamber. The coverslip was coated with 7 mg/ml lectin with a method adapted from Babashak and Phillips (1989). After 8–10 min, the solution in the recording chamber was exchanged for standard, glucose-containing bathing solution that now also contained bovine serum albumin (0.1 mg/ml) and nifedipine (10 μM).

The recording chamber was held on the stage of an inverted microscope equipped with DIC optics. Cells were observed under infrared illumination (860–920 nm) with the aid of a video camera and monitor. The recording chamber held ~0.5 ml of bathing solution, and it was intermittently perfused at 1–2 ml/min. All experiments were carried out at room temperature (20–22°C). Membrane currents under voltage clamp were measured with a patch clamp amplifier, as previously described (Miller and Korenbrot, 1993*b*). Analogue signals were low pass filtered with 50 Hz cut off and digitized on line at 333 Hz with 12-bit accuracy (Fastlab System, Indec Inc., Capitola, CA). Numerical solution of differential equations and simulations were carried out using Tutsim (Tutsim Products, Palo Alto, CA) and curve fitting was executed with a nonlinear, least-squares minimization algorithm (NFIT, Island Products, Galveston, TX). The statistical error in averaged data is presented as standard deviation (SD) throughout this report.

Conventional Whole-Cell Recording

Membrane currents were recorded with tight-seal electrodes produced from Corning 1724 glass (aluminosilicate, 1.5/1.0 mm o.d./i.d.) with typical tip opening of 0.8 to 1 μm (tip resistance 5 to 7 MΩ). In studies with whole rods, electrodes were sealed onto the inner segment. In studies of detached rod outer segments, the electrodes were sealed onto the side of the organelle. In conventional whole-cell mode, tight-seal electrodes were filled with a solution of the following composition (in millimolar): K gluconate (58), K-aspartate (20), KCl (20), $MgCl_2$ (4), $ATPNa_2$ (3), $GTPNa_3$ (1), MOPS (15), pH 7.25, 228 mosM osmotic pressure. We will refer to this solution as TSIS (tiger salamander intracellular solution). The free Mg concentration was calculated to be 0.5 mM. The free Ca^{2+} concentration in TSIS was between 200 and 500 nM, as measured with Fura2 in a spectrofluorimeter. To obtain the desired free Ca^{2+} concentration careful attention was paid to the production of TSIS. Only plasticware was used and a solution containing all components except $MgCl_2$ was made free of all multivalent cations by passage over a column of Chelex 100 (Bio-Rad Laboratories). Ultrapure $MgCl_2$ (99.9999% pure, Aldrich Chemical Co., Milwaukee, WI) was then added and the solution stored in small aliquots at −20°C.

In some experiments, TSIS was modified as follows: (*a*) Hi Na-TSIS, a TSIS solution in which Na-aspartate replaced K-aspartate in equimolar amounts and NaCl replaced 10 mM KCl isoosmotically; (*b*) TSIS-BAPTA, a TSIS solution containing 5 mM BAPTA and titrated to a final free Ca^{2+} concentration of 270 nM with the aid of a Ca^{2+}-sensitive electrode; (*c*) Hi Na-TSIS-BAPTA, Hi Na-TSIS solution containing 5 mM BAPTA and 270 nM free Ca^{2+} concentration. When any of these solutions were used, the electrical behavior of both whole rods and detached outer segments stabilized only 2–5 min after first achieving whole-cell mode. Presumably, this interval was required for the cell's cytoplasm to come to equilibrium with the solution in the tight-seal electrode. We routinely assessed whether the rod's response had stabilized by monitoring in darkness the current activated by 8.65-s pulses to +60 mV presented at 25-s intervals beginning after first rupturing the membrane patch. Data reported here were those collected in the steady state.

Whole-Cell Recording with the Perforated-Patch Method

For experiments in the perforated-patch mode (Horn and Marty, 1988), we filled the front of the electrode with the following solution (in millimolar): K gluconate (85), KCl (20), NaCl (9), $MgCl_2$ (0.5) MOPS (15), pH 7.25, 228 mosM osmotic pressure. We filled the back of the electrode with the same solution containing, in addition, pluronic F-127 (400 μg/ml) and amphotericin B (112.5 μg/ml). In some experiments, nystatin (100 μg/ml) replaced Amphotericin B with comparable results. To prepare the backfilling solution, appropriate aliquots of pluronic F-127 (200 mg/ml) and amphotericin B (30 mg/ml) in anhydrous DMSO were added to 500 μl of the solution and sonicated for 60 s in a bath sonicator (80 W). 250 μl of this sonicate were then added to 250 μl of fresh solution and sonicated again for 60 s. The sonicate was used within 90 min of preparation. The amphotericin B stock in DMSO was kept shielded from light at −20°C for periods of up to 5 d and the pluronic F-127 stock was kept at room temperature for periods of up to 2 wk. Our procedure is a modification of the original method of Horn and Marty (1988), based on suggestions made by Sala, Parsey, Cohen, and Matteson (1991) and by Rae, Cooper, Gates, and Watsky (1991). On occasion, the perforated patch can spontaneously convert into a conventional whole-cell recording. In our experiments, this problem was evident by the rapid loss of photocurrent because the solution filling the tight-seal electrode lacked ATP and GTP. If such conversion occurred, we abandoned the cell.

Photostimulation

Stimuli of unpolarized light were presented to the entire photoreceptor through the objective of the microscope used for viewing the cells. We stimulated with flashes 20 ms in duration at 520 nm as selected with a narrow band interference filter (±10 nm half band width). Light intensity was controlled with neutral density filters and was measured with a calibrated photodiode (United Detector Technology, Santa Monica, CA) placed on the microscope stage in the position of the recording chamber.

RESULTS

We undertook the present study to investigate in rod photoreceptors the voltage dependence of the outer segment current in darkness. We reasoned that analysis of this current and comparison with results we previously obtained in cones (Miller and Korenbrot, 1993*b*) might help us understand the functional differences between receptor types. We measured voltage-clamped membrane currents in whole rods and in detached rod outer segments isolated from tiger salamander retinas. We defined the outer segment current in whole rods at each voltage as the difference between

currents measured in darkness minus those measured under continuous, bright 520 nm light (typically, 1.5×10^6 photons $\mu m^{-2} s^{-1}$). To reduce the contribution of inner segment currents to the total currents measured, we conducted all measurements in the presence of 10 μM nifedipine; this blocker eliminated the voltage-dependent Ca^{2+} current and the Ca^{2+}-dependent Cl current known to exist in tiger salamander rod inner segments (Bader, Bertrand, and Schwartz, 1982; Corey, Dubinsky, and Schwartz, 1984). Nifedipine was without effect on the outer segment current as evidenced by the findings that: (*a*) the photocurrents were the same in the presence and absence of nifedipine (see Fig. 1), and (*b*) the properties of the outer segment current measured in whole rods in the presence of Nifedipine were similar to those measured in detached outer segments in the absence of the Ca^{2+} channel blocker.

Photocurrents Recorded Using the Perforated-Patch Method

As we document below, the features of the voltage-dependent outer segment currents depend on the ionic composition of the cytoplasm. To determine the electrical

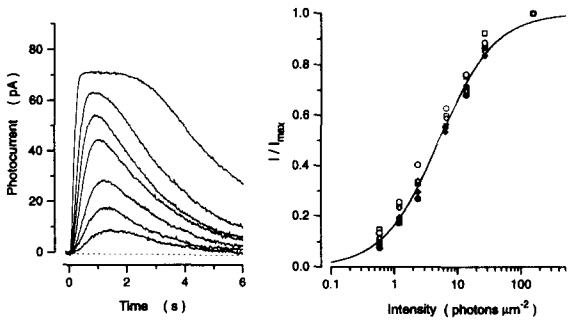

FIGURE 1. Photocurrents measured with the perforated-patch technique in dark-adapted whole rods at room temperature. 20-ms flashes of 520 nm light were presented at time zero. Shown are responses elicited by flashes of the following intensity (in photons μm^{-2}): 0.59, 1.21, 2.38, 6.53, 13.72, 27.42, and 156.67. On the right are shown normalized peak photocurrent amplitudes measured in six different rods, each identified by a distinct symbol, at various light intensities. The continuous line is a least square fit of the Michaelis-Menten function to the data points. The intensity necessary to half-saturate the current amplitude was, on average, 3.56 ± 1.9 photons μm^{-2} (n = 19).

properties of the outer segment under the least possible experimental perturbation, we studied whole rods using the perforated-patch mode of whole-cell recording (Horn and Marty, 1988). We generally used amphotericin B, but we also used nystatin with indistinguishable results. Control experiments demonstrated that the agents used to dissolve and stabilize the ionophores in the electrode-filling solution had no physiological effect of their own (DMSO, final concentration 1.25% vol/vol and pluronic F-127, final concentration 0.12% wt/vol). To produce perforated patches, we first obtained giga seals and then continuously monitored membrane capacitance to determine the moment that whole-cell mode was attained. We typically attained whole cell mode 4–7 min after giga seal formation. The capacitance of whole rods measured with the perforated patch was, on average, 18.1 ± 2.8 pF (n = 32). Conventional whole cell recordings yielded an average capacitance of 18.8 ± 3.1 pF (n = 31).

Fig. 1 illustrates typical photocurrents measured in dark-adapted whole rods with the perforated-patch technique. Average peak photocurrent was 72.9 ± 16.5 pA

(n = 20). The dependence of the peak photocurrent on light intensity was well described by the Michaelis-Menten function, with half saturation at an average intensity of 3.6 ± 1.9, photons μm^{-2} (n = 19) (Fig. 1). The time to peak for dim light responses, those with peak amplitude less than 20% that of the saturated amplitude, was 1430 ± 257 ms (n = 13). The flash sensitivity was 0.91 ± 0.52 pA/photoisomerization, calculated assuming a cross-section of absorption of 22.7 μm^2 for tiger salamander rods.

Dark, Voltage-activated Currents in the Rod Outer Segment

Fig. 2 illustrates membrane currents measured in a whole rod with the perforated-patch method. The data are typical of the rods studied with this protocol (n = 9). The

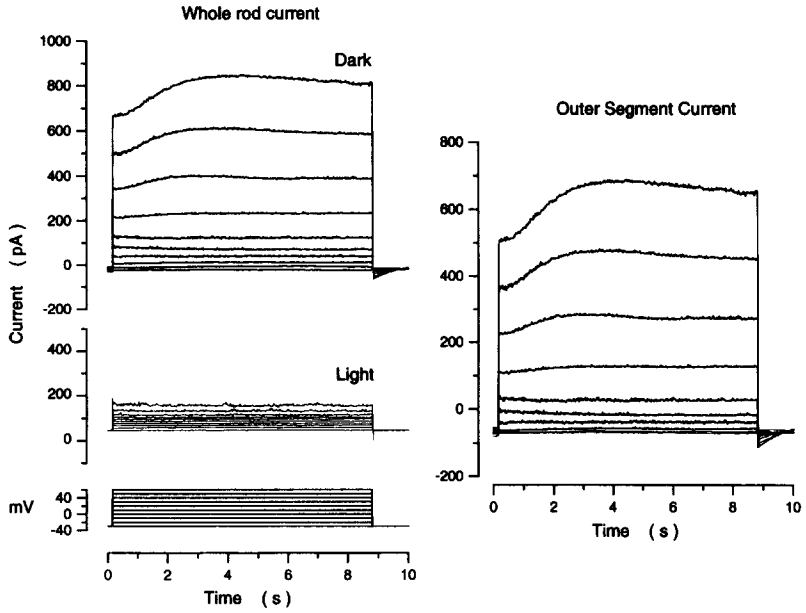

FIGURE 2. Voltage-dependent membrane currents measured in a whole rod with the perforated-patch technique. Left illustrates currents measured either in the dark (*top*) or under bright, continuous illumination (520 nm light, 1.5 × 10^6 photons μm^{-2} s^{-1}) (*bottom*). Right illustrates dark, outer segment-specific currents determined from the difference between currents measured in darkness and those measured in the light. Membrane voltage was held at −30 mV and 8.65 s duration voltage steps between −30 and +60 mV, in 10-mV increments, were presented at 20-s intervals. Voltages ≥ +20 mV activated the outer segment current with a sigmoidal time course. We call this DVAC (dark, voltage-activated current).

cell was held at −30 mV and was depolarized for 8.65 s to voltages in the range between −30 and +60 mV in 10-mV steps. Depolarizing steps were presented at 20-s intervals. We measured currents first in complete darkness and then in the presence of continuous illumination that saturated the photocurrent amplitude. We computed the outer segment-specific currents from the difference between the currents measured in darkness minus those measured in the light. The currents measured in the

light are inner segment-specific currents that arise from the activity of various time- and voltage-dependent channels present in this membrane (Bader et al., 1982; Corey et al., 1984). At −30 mV and in the dark, the total membrane current was −6.7 ± 15.9 pA (n = 9), the sum of a net inward current through the outer segment and a net outward current through the inner segment (Hagins, Penn, and Yoshikami, 1971).

In darkness, the outer-segment current was inward and time independent for voltages between −30 and +10 mV (Fig. 2). The current reversed direction above +10 mV and it exhibited a time-dependent activation for voltages ≥ +20 mV. Current activation had a sigmoidal time course and the kinetics and extent of activation changed with voltage (Fig. 2). We call this current DVAC. For all cells measured, currents activated by depolarizations to +60 mV reached their maximum value 4–6 s after the onset of depolarization and the maximum current enhancement was, on average, 1.28-fold the initial current (Table I). Since the plasma membrane in

TABLE I

*Ratio of Enhanced to Initial Conductance under Various Conditions of Experimental Recording**

	Perforated patch	WCR with TSIS‡		WCR with Hi Na-TSIS	WCR with BAPTA‖
V_m	Whole rod (10§)	Whole rod (8)	dROS (8)	Whole rod (7)	Whole rod (12)
	g_{max}/g_{init}	g_{max}/g_{init}	g_{max}/g_{init}	g_{min}/g_{init}	g_{max}/g_{init}
+30	1.13 ± 0.08	1.10 ± 0.02	1.34 ± 0.10	0.57 ± 0.21	0.87 ± 0.15
+40	1.17 ± 0.09	1.14 ± 0.05	1.57 ± 0.18	0.44 ± 0.24	0.87 ± 0.14
+50	1.23 ± 0.09	1.22 ± 0.10	1.74 ± 0.28	0.34 ± 0.25	0.90 ± 0.18
+60	1.28 ± 0.11	1.23 ± 0.12	1.76 ± 0.30	0.28 ± 0.23	0.87 ± 0.13

*Values listed are the ratio of the maximum (or minimum) conductance at a given voltage over the conductance measured 60 ms after the onset of depolarization.

‡Conventional whole-cell recording.

§Number of cells, average ±SD.

‖This average includes both TSIS and Hi Na-TSIS solutions containing BAPTA.

the outer segment contains only one class of ion channels, those gated by cGMP (Baylor and Lamb, 1982; Baylor and Nunn, 1986; Hestrin and Korenbrot, 1987), our results suggest that depolarization in the dark specifically activates these channels.

Electrical Properties of DVAC in Whole Rods

We tested the thesis that DVAC arises from voltage-dependent activation of the cGMP-gated conductance, and not from activation of a previously unrecognized class of outer segment channels, by comparing the *I-V* curves and reversal potential of the photocurrent with those of DVAC. We measured currents in whole rods with the perforated patch method. To determine the *I-V* curve of the photocurrent, voltage was held at −30 mV and currents were first activated in the dark by 8.65 s step depolarizations in the range between −30 and +60 mV in 10-mV steps. In the same cell, the depolarizing series was then repeated and a flash of light was presented 300 ms after the onset of the voltage step (Fig. 3). Finally, the cell was exposed to

continuous light and the depolarizing series repeated again. At each voltage, the photocurrent amplitude was determined by subtracting the peak photocurrent from the current amplitude measured in the dark at the same voltage and at the same point in time. The DVAC current amplitude at each voltage was determined by subtracting from the maximum current in the dark the current measured at the same time point under continuous illumination. Fig. 3 illustrates currents and *I-V* curves for one cell that is typical of the 11 cells studied with this protocol.

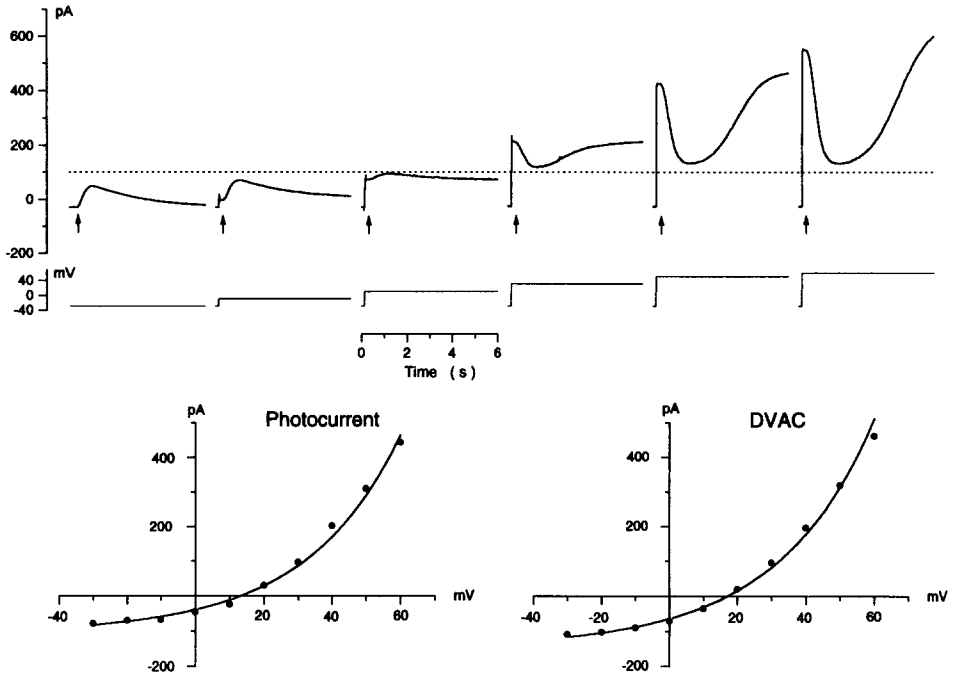

FIGURE 3. Voltage- and light-dependent outer segment currents in a whole rod studied with the perforated-patch technique. The upper tracings illustrate currents generated by step depolarizations from −30 mV holding voltage to −30, −10, +10, +30, +50, and +60 mV. 300 ms after the voltage step onset, a 20 ms flash of 520 nm light was presented that delivered 13.7 photons μm^{-2}. The lower panels are the *I-V* plots of the photocurrents (*left*) or of DVAC (*right*) in this rod. The continuous lines are least square fits of Eq. 1 to the data points. The values of the adjustable parameters in Eq. 1 that best fit the data shown were, for photocurrents γ = 0.03, Vr = −12.54 mV, Vo = 25.9 mV; for DVAC γ = 0.03, Vr = −12.44 mV, Vo = 26.0 mV.

The photocurrent *I-V* data were well fit by the empirical function:

$$I(V) = A_1 \exp\left((1-\gamma)\left(\frac{V-V_r}{V_o}\right)\right) + A_2 \exp\left((-\gamma)\left(\frac{V-V_r}{V_o}\right)\right) \quad (1)$$

where A_1 and A_2 are current amplitudes and γ, V_r, and V_o are adjustable parameters. This function fits photocurrent data in many vertebrate photoreceptors (review in Yau and Baylor, 1989). Nonlinear, least-squares fits of Eq. 1 to data from 11 rods had

the following average values $\gamma = 0.039 \pm 0.019$, $V_r = -12.4 \pm 0.1$ mV and $V_0 = 26.1 \pm 0.1$ mV. Examination of the data in Fig. 3 reveals that depolarization has profound effects on the kinetics and sensitivity of the photocurrent, not just its amplitude. Although we do not examine these effects in detail here, it is worth emphasizing that, in general, the photocurrent slowed down in time course as the voltage depolarized. While the slowdown was more remarkable on the recovery phase of the photoresponse, the activation phase also slowed down as the membrane depolarized. We have observed the same qualitative effects in cones (Miller and Korenbrot, 1993*b*).

The *I-V* data of DVAC were also very well fit by Eq. 1 (Fig. 3). The optimized fit of Eq. 1 to DVAC measured in 12 different rods had the following average values: $\gamma = 0.027 \pm 0.017$, $V_r = -13.0 \pm 1.6$ mV and $V_0 = 26.3 \pm 0.7$ mV. That is, the *I-V* curve of the photocurrent and of DVAC are the same. Of greater significance was the fact that the reversal potentials of the light-sensitive current: 14.8 mV ± 2.5 ($n = 11$), and DVAC: 16.7 ± 6.0 ($n = 12$) were also the same. Thus, DVAC and the photocurrent must arise from the activity of precisely the same ion channels.

DVAC in Detached Rod Outer Segments

We confirmed that voltage-dependent changes in outer segment currents measured in whole rods arise from changes in the activity of the light-sensitive conductance by demonstrating that detached rod outer segments (dROS) also exhibit DVAC (Fig. 4). Using tight-seal electrodes in the conventional whole-cell recording mode, these organelles can support phototransduction, provided that GTP and ATP are supplied by the pipette filling solution (Hestrin and Korenbrot, 1987; Rispoli, Sather, and Detwiler, 1993). As expected, dROS studied with the perforated-patch technique do not exhibit photoresponses or a standing current in the dark (data not shown). On the other hand, dROS studied with TSIS-filled electrodes under conventional whole-cell recording developed a stable dark current and typical photoresponses in the course of the first 3–5 min after rupture of the membrane under the electrode tip. In eight dROS the average holding current in the dark at −30 mV was −36.6 ± 12.2 pA (inward current). With dROS held at −30 mV, we investigated the effects of 8.65-s depolarizing steps between −30 and +60 mV in 10-mV increments. As we illustrate in Fig. 4, dROS in the dark exhibited stable DVAC currents that were entirely suppressed by continuous, bright illumination. In the light, currents were extremely small, with an average membrane slope resistance $\geq 4.79 \pm 3.6 \times 10^9\ \Omega$ ($n = 5$) at +60 mV. This result confirms the original finding of Baylor and Lamb (1982) (also Baylor and Nunn [1986] and Hestrin and Korenbrot [1987]) that outer segment membranes contain only light-sensitive channels.

The *I-V* curve of DVAC in dROS was well described by the empirical function given as Eq. 1, and it is essentially the same that describes the *I-V* curve of DVAC in whole rods (Fig. 4). In eight different dROS we measured the *I-V* curve of DVAC both 60 ms after the onset of the depolarization, an early point, and later, at the maximum of the enhanced current (4.7 − 6.3 s). The average values of the adjustable parameters that best fit the data were, for early point: $\gamma = -0.029 \pm 0.05$, $V_r = -14.2 \pm 5.7$ mV and $V_0 = 25.8 \pm 2.6$ mV and for late point: $\gamma = -0.15 \pm 0.10$, $V_r = -12.0 \pm 1.4$ mV and

V_o = 24.8 ± 0.4 mV. The average reversal potential was the same for early points and late points: 11.0 mV ± 1.0.

To analyze the voltage dependence of DVAC activation we measured in dROS the difference between the initial current amplitude, 60 ms after the voltage step onset, and the amplitude of the maximum current activation at that voltage. Because currents were measured at a constant voltage, this difference is a direct measure of

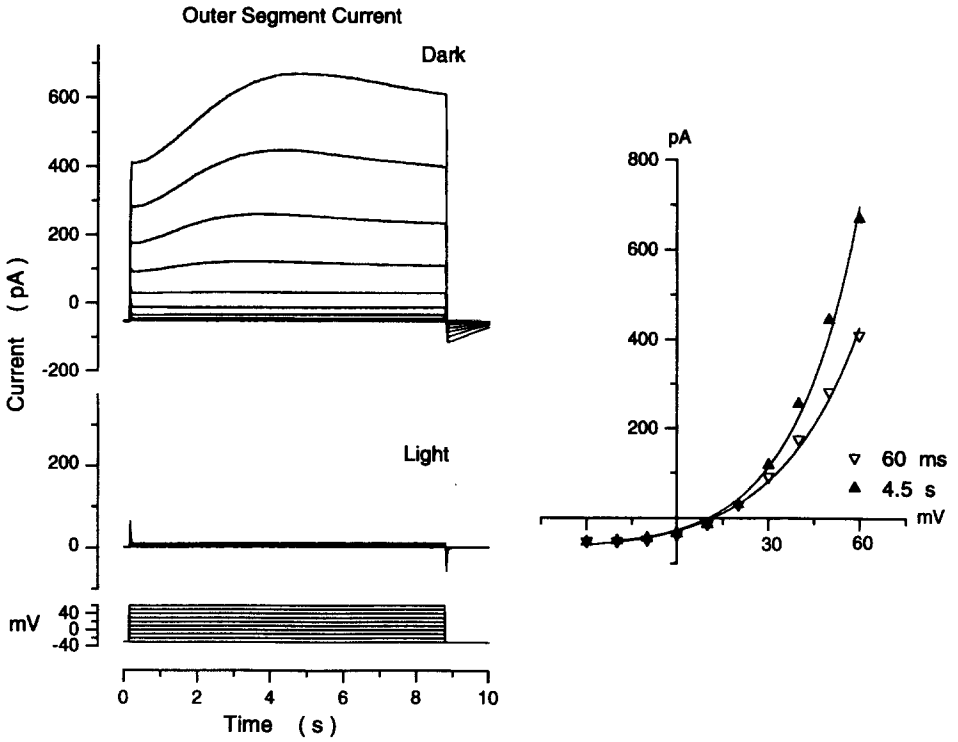

FIGURE 4. Voltage-dependent membrane currents measured in a detached rod outer segment with a tight-seal electrode filled with TSIS. Left illustrates currents measured either in the dark (*top*) or under bright, continuous illumination (520 nm light, 1.5 × 10^6 photons μm^{-2} s^{-1}; *bottom*). Membrane voltage was held at −30 mV and 8.65 s duration voltage steps between −30 and +60 mV, in 10-mV increments, were presented at 20-s intervals. In the dark, the detached outer segment exhibits DVAC. Right illustrates the *I-V* curve of DVAC measured either 60 ms or 4.5 s after the onset of the step depolarization. The continuous lines are least square fits Eq. 1 to the data points.

the conductance enhancement underlying DVAC. For voltages between −30 and +10 mV there was no conductance enhancement (Fig. 4). Above +10 mV, the conductance enhancement increased with voltage, and this dependence was well described by the Boltzman equation:

$$\frac{\Delta g(V)}{\Delta g_{max}} = \left(1 + \exp\left(\frac{V - V_o}{k}\right)\right)^{-1} \quad (2)$$

where $\Delta g(V)/\Delta g_{max}$ is the normalized conductance enhancement, V_o is the membrane voltage at the midpoint of activation and k describes the steepness of the voltage dependence. For eight dROS, the best fit of the function to experimental data yielded the following average values for these constants V_o = 31.5 mV ± 0.7, k = 6.1 ± 0.6.

Although the *I-V* curves of DVAC measured in dROS and in whole rods were nearly identical, indicating that the current activation reflects a specific increase in the cGMP-gated conductance, the extent of the activation was not the same. We measured the magnitude of activation at each voltage as the ratio of the maximum activated current over the initial current amplitude, measured 60–80 ms after the onset of the depolarizing voltage. The results of these measurements are presented in Table I. They indicate that, at each voltage tested, dROS exhibited slightly larger activation than that observed in intact rods with perforated patches. Conventional whole-cell recordings in whole rods using TSIS-filled electrodes also displayed DVAC. These currents were similar to those measured with the perforated-patch technique (Table I). The differences in the quantitative features of DVAC between intact cells and dROS are likely to reflect the effects of variation in the ionic composition of the cytoplasm. In dROS the cytoplasmic ionic composition is probably closer to that of the electrode filling solution than in whole rods studied with conventional whole-cell recordings because the diffusional access between electrode and outer segment is less restricted and the buffering effects of mitochondria are absent (Hestrin and Korenbrot, 1987; Rispoli et al., 1993). Data measured with the perforated-patch techniques should more nearly reflect the intact condition in rods.

The Effects of Extracellular Ca^{2+} on DVAC

To confirm that the features of DVAC in the intact rod are sensitive to the cytoplasmic ionic composition, we investigated the effects of varying extracellular Ca^{2+} concentration on DVAC recorded using the perforated patch method. At constant holding voltage, lowering extracellular Ca^{2+} in the dark decreases its cytoplasmic concentration, and raising it increases the cytoplasmic Ca^{2+} (Lamb and Matthews, 1988). We changed the solution bathing the cell under study with test solutions that flowed from a 100-μm diam glass capillary placed ~150 μm away from the cell.

Fig. 5 illustrates currents measured in the same rod with the perforated-patch technique in the presence of varying extracellular Ca^{2+} concentrations. In the dark, membrane voltage was held at −30 mV and 8.65-s step depolarizations to +60 mV were repeatedly delivered at 20-s intervals. Outer segment currents, determined from the dark-light difference currents, were measured first in 1 mM Ca^{2+}, then in 0.1 mM Ca^{2+} and then again upon returning to 1 mM Ca^{2+}. In 1 mM external Ca^{2+} in the dark the outer segment currents exhibited a stable DVAC. Lowering extracellular Ca^{2+} increased the outer segment membrane conductance as reflected both by an increase in the holding current and in the initial amplitude of the current upon depolarization. Also, the extent of conductance activation underlying DVAC was much larger in 0.1 mM Ca^{2+} than in 1 mM Ca^{2+}, although its time course was nearly unchanged. The enhancement in conductance under DVAC was also apparent in the much larger tail current amplitude measured under low Ca^{2+}. The same results were

obtained in all cells tested with this protocol. The average holding current in 0.1 mM Ca^{2+} was -144.7 ± 52.0 pA and the average conductance enhancement under DVAC at +60 mV was 1.66 ± 0.21 fold ($n = 6$). Upon return to normal Ca^{2+}, the outer segment currents recovered their initial characteristics, but only transiently. As time progressed, the outer segment currents continued to change in time course; they became slightly inactivating and light insensitive within 5–10 min. The changes in the quantitative features of DVAC upon changes in extracellular and, presumably, intracellular Ca^{2+} are qualitative evidence of the sensitivity of these currents to the ionic composition of the rod outer segment cytoplasm.

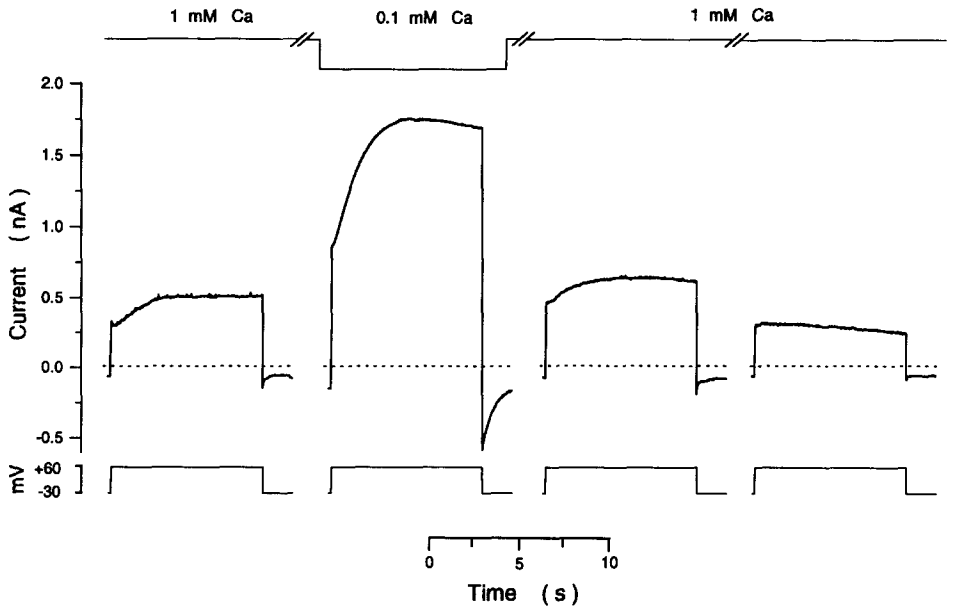

FIGURE 5. Effects on the features of DVAC of changes in extracellular Ca^{2+} measured in whole rods with the perforated-patch technique. Shown are outer segment currents generated in darkness in response to step depolarizations to +60 mV. Currents were first measured in the standard bathing solution containing 1 mM Ca^{2+}, then in a solution containing 0.1 mM Ca^{2+} and then again upon returning to the standard solution. The amplitude of DVAC was significantly enhanced by lowering extracellular Ca^{2+}. Upon returning to normal Ca^{2+}, the cell exhibited DVAC similar to that first measured in 1 mM Ca^{2+}. In time, DVAC transformed to a current that exhibited a small inactivation.

Dark, Voltage-inactivated Currents in Rod Outer Segment

Baylor and Nunn (1986) observed in tiger salamander rods that depolarization in the dark to voltages $\geq$ +20 mV inactivated the outer segment current with an exponential time course. The extent and time course of inactivation were voltage dependent. We call these currents DVIC (dark, voltage-inactivated current). Because the features of DVAC are sensitive to ionic cytoplasmic composition, we reasoned that

DVIC reported by Baylor and Nunn (1986) might have arisen from unintended changes in cytoplasmic composition of the rod outer segment in their experiments. Because they voltage clamped the rods using conventional microelectrodes, it is possible, for example, that the electrode puncture allowed loading of ions abundant in the bathing medium, but not in the cytoplasm, such as Ca^{2+} or Na^{+}. Therefore, we investigated the effects of cytoplasmic Na^{+} on the rod outer segment currents with conventional whole-cell recordings using tight-seal electrodes filled with Hi Na-TSIS.

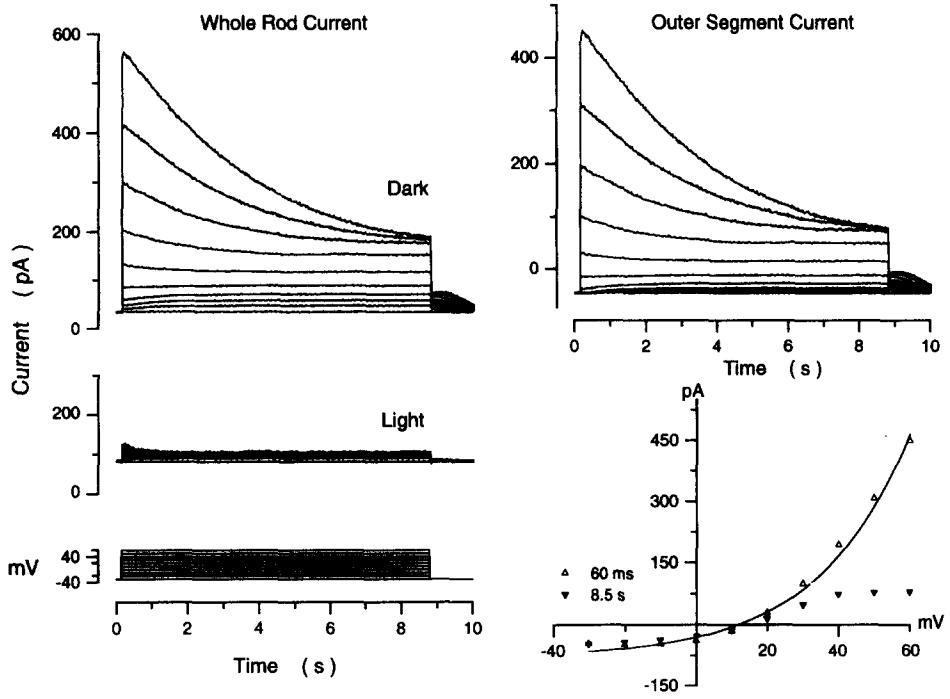

FIGURE 6. Voltage-dependent membrane currents measured in a whole rod with a tight-seal electrode filled with Hi Na-TSIS. Left illustrates currents measured either in the dark (*top*) or under bright, continuous illumination (520 nm light, 1.5×10^6 photons μm^{-2} s^{-1}; *bottom*). Right illustrates dark, outer segment-specific currents determined from the difference between currents measured in darkness and those measured in the light. Voltages $\geq$ +20 mV inactivated the outer segment currents with an exponential time course. We call this current DVIC and its current-voltage characteristic is illustrated in the panel. Initial current amplitude was measured 60 ms after the onset of depolarization. Maximally inactivated currents were measured 8.5 s after the onset of depolarization. The continuous line is a least square fit of Eq. 1 to the experimental points with $\gamma = 0.005$, $Vr = 12.51$ mV and $Vo = 25.05$ mV.

In the presence of Hi Na-TSIS, outer segment currents demonstrated in the dark a time-dependent inactivation at all voltages (DVIC) (Fig. 6). Hi Na-TSIS contained 39 mM, rather than the normal 9 mM. The average holding current was 15.8 ± 13.2 pA (n = 19). The average saturated photocurrent amplitude at −30 mV was 44.9 ± 16.5 pA. That is, the holding current was more positive and the photocurrent amplitude

smaller than the values measured in intact rods with perforated patches. For step voltages under +20 mV, the inactivation was small and its time course was well fit by a single exponential, but the rate and extent of inactivation changed with voltage (Fig. 6). We measured the extent of inactivation as the ratio of the current amplitude at the end of the pulse (8.5 s) over the amplitude measured 60 ms after the onset of the depolarizing voltage. Table I presents average inactivation measured at various voltages. Although Baylor and Nunn (1986) did not analyze in detail the characteristics of DVIC, inspection of their published records show that the features of our data are similar to theirs. dROS studied with Hi Na-TSIS exhibited DVIC similar to that observed in whole rods (data not shown).

We explored the electrical properties of DVIC. To determine its *I-V* curve we measured, at each voltage tested, the difference in amplitude between currents in the dark and under continuous illumination. We measured the *I-V* curve at two time points: 60 ms after the onset of the depolarizing voltage, and 8.5 s after the voltage onset (Fig. 6). The curve measured at the early time point was, again, well fit by Eq. 1 with average values in six cells of: $\gamma = 0.017 \pm 0.02$, $V_r = -12.3 \pm 0.3$ mV and $V_o = 26.6 \pm 2.5$ mV with a reversal potential of 11.5 ± 1.2 mV. The *I-V* curve measured for late points was not fit by Eq. 1. The late curve overlapped the early one at voltages $\leq +20$ mV and it had the same reversal potential. However, for larger depolarizations the late conductance was severely reduced and the currents were small. The near identity of the *I-V* curves and reversal potentials of DVIC to those of the photocurrent, and the finding that dROS studied with Hi Na-TSIS also display light-suppressible DVIC currents, affirm that DVIC, like DVAC, arises from the activity in the dark of the cGMP-gated channels. DVIC, however, reflects a voltage-dependent closing of the channels, whereas DVAC reflects additional channel opening.

Outer segment tail currents were different in rods that exhibited DVAC from those in rods that manifested DVIC. Under DVAC, tail currents that followed depolarizing voltages $\geq +20$ mV had an instantaneous value that was more negative than that of the original holding current and decayed with a single exponential time course back to the original holding current (Fig. 2). This electrical behavior indicates that under DVAC, a large number of cGMP-gated channels were open at the end of the depolarizing pulse and they then slowly closed as the voltage was held at −30 mV. Under DVIC conditions, in contrast, the tail currents had an instantaneous value that was more positive than the original current level (Fig. 6). The tail currents slowly grew from their instantaneous value back to the original holding current (Fig. 6). This behavior revealed that under DVIC, most cGMP-gated channels were closed at the end of the depolarizing pulse and they then slowly reopened when the voltage was returned to −30 mV.

Effects of Cytoplasmic BAPTA

The activity of the cGMP-gated channels in tiger salamander rods is not voltage dependent (Zimmerman and Baylor, 1986; Haynes, Kay, and Yau, 1986; Karpen, Zimmerman, Stryer, and Baylor, 1988). Therefore, DVAC and DVIC must arise from a voltage-dependent process that modulates the concentration of cGMP in the dark, but not from direct control of the channel activity by voltage. In cones we suggested

and tested a simple mechanism to explain DVAC (Miller and Korenbrot, 1993*b*). In this mechanism (see below), changes in membrane voltage are linked to channel opening through changes in cytoplasmic Ca^{2+} concentration. To test experimentally the importance of changes in cytoplasmic Ca^{2+} in the mechanism of DVAC and DVIC, we investigated the effects on these currents of BAPTA loaded into whole rods through the tight-seal electrode in conventional whole-cell mode. If changes in membrane voltage are linked to regulation of cGMP through changes in cytoplasmic Ca^{2+} concentration, then DVAC and DVIC should be strongly attenuated or even abolished in the presence of the Ca^{2+} buffer.

We tested both TSIS and Hi Na-TSIS solutions containing 5 mM BAPTA titrated to yield 270 nM free Ca^{2+} concentration, a value near the resting Ca^{2+} concentration in dark-adapted rods (Korenbrot and Miller, 1989). We confirmed that BAPTA was indeed loaded into the outer segment cytoplasm by verifying that photocurrents exhibited features characteristic of the action of the buffer; the time course of the photocurrents slowed down and large oscillations occurred at the end of the photoresponse (data not shown) (Korenbrot and Miller, 1986; Lamb et al., 1986; Matthews, 1991). In the presence of BAPTA, outer segment currents generated by depolarization in darkness were essentially time independent at all voltages. Fig. 7 illustrates outer segment currents measured in whole rods loaded with either TSIS-BAPTA or Hi Na-TSIS-BAPTA. Depolarization with the typical pulse protocol did not produce a rapid sigmoidal enhancement or an exponential decline in current amplitude, respectively. Ratios of current amplitudes at the end and the beginning of the voltage pulse were ~0.9 at all voltages for 12 cells tested with TSIS (n = 8) or Hi Na-TSIS (n = 4) (Table I). Fig. 7 demonstrates that the tail currents in the presence of BAPTA were also time independent. Yet, the cGMP-gated channels themselves were unaffected by the buffer because the shape of the *I-V* curves of the dark outer segment currents and their reversal potential were the same in buffered and unbuffered cells (Fig. 7). In 10 BAPTA-loaded rods, the *I-V* curves of outer segment currents measured 60 ms after the onset of the voltage pulse were well fit by Eq. 1 with average values: $\gamma = 0.022 \pm 0.029$, $V_r = -12.4 \pm 2.8$ mV and $V_o = 24.7 \pm 0.6$ mV and a reversal potential of 12.5 ± 3.8 mV. Thus, a voltage-dependent change in cytoplasmic Ca^{2+} concentration is a *requisite* step in the process that generates either DVAC or DVIC.

We observed one difference in the electrical behavior of whole rods studied with TSIS-BAPTA or Hi Na-TSIS-BAPTA: Outer segment dark current was stable in TSIS-BAPTA loaded rods, but it grew progressively smaller in amplitude and, eventually, vanished in rods loaded with Hi Na-TSIS-BAPTA. Elimination of the outer segment currents suggests that rod outer segment are unable to maintain their normal ionic composition when Ca^{2+} homeostasis and the function of the $Na^+/Ca^{2+},K^+$ exchanger are compromised by abnormally high internal Na^+.

Differences in DVAC between Rods and Cones

The quantitative features of DVAC in rods are profoundly different from those in cones. Fig. 8 illustrates, side by side, outer segment currents generated in darkness by depolarization of either tiger salamander rods or striped bass single cones. Currents in rods were measured with the perforated-patch method, while those in cones were

measured with suction electrodes while controlling membrane voltage with conventional tight-seal electrodes (Miller and Korenbrot, 1993*b*). Inspection of the data shows that at any voltage ≥ +20 mV, DVAC is slower and smaller in rods than cones. To facilitate comparison, we converted current into conductance and then normalized the data such that the initial conductance at +20 mV was unity in both cell types (Fig. 8). Conductance was computed by dividing current by electromotive force, since

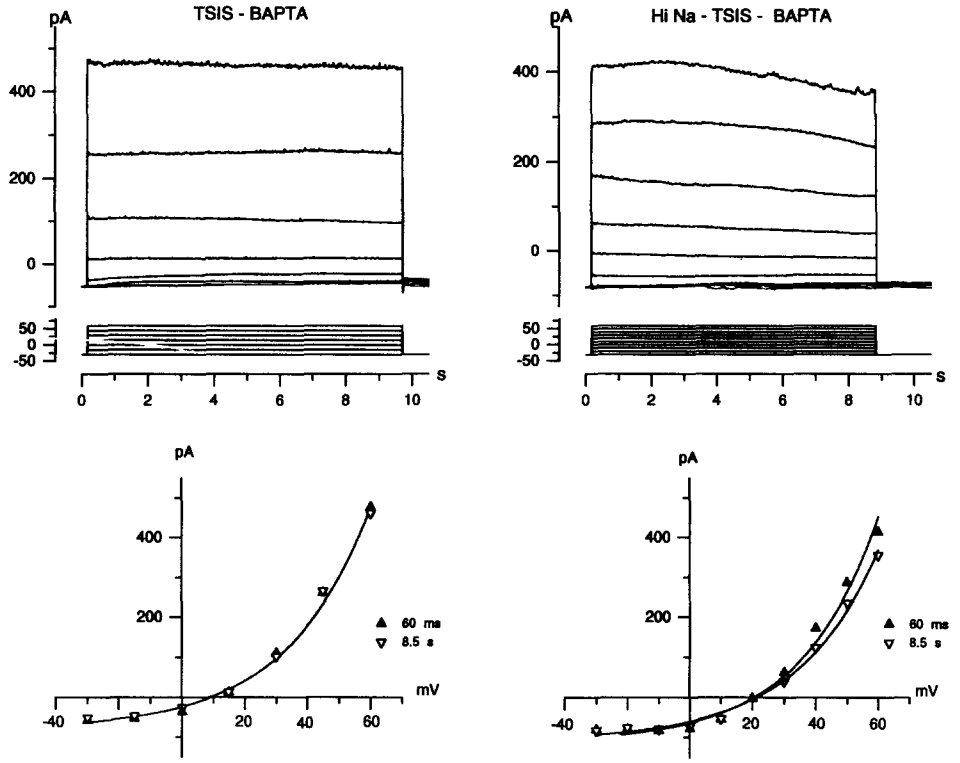

FIGURE 7. Effect of 5 mM cytoplasmic BAPTA on DVAC and DVIC. The left shows data measured in a whole rod with a tight-seal electrode containing TSIS with 5 mM BAPTA and 270 nM free Ca^{2+}. Membrane voltage was held at −30 mV and 8.65-s duration voltage steps between −30 and +60 mV, in 15-mV increments, were presented at 20-s intervals. The currents at all voltages were essentially time independent, that is, DVAC was abolished. The *I-V* curves determined either 60 ms or 8.5 s after the onset of depolarization were identical, as shown in the bottom. The continuous line in the *I-V* plot is a least squares fit Eq. 1 to the data points with $\gamma = 0.03$, $Vr = 12.51$ mV and $Vo = 24.8$ mV. The right illustrates data measured in a whole rod with a tight-seal electrode containing Hi Na-TSIS with 5 mM BAPTA and 270 nM free Ca^{2+}. Membrane voltage was held at −30 mV and 8.65 s duration voltage steps between −30 and +60 mV, in 10-mV increments, were presented at 20-s intervals. The expected DVIC was strongly attenuated, and only at the highest voltages did we observe a small inactivation. The bottom shows the *I-V* curve measured either 60 ms or 8.5 s after the onset of depolarization. The two curves deviated from each other slightly at large depolarizations. The continuous lines are best fits Eq. 1 to the data points.

the reversal potential of the outer segment currents was known in each cell. Table II presents a comparison of DVAC data averaged from measurements in 9 cones and 10 rods. Cone data were taken from our previous publication (Miller and Korenbrot, 1993*b*). Current enhancement at each voltage was defined as the ratio of the maximum value of the current over its initial value, measured 60 ms after the onset of depolarization. Although DVAC has a sigmoidal time course, for purposes of comparison we measured the time elapsed between the voltage change and the point at which currents reached 63% ($1-1/e$) of their maximum value. Data in Fig. 8 and

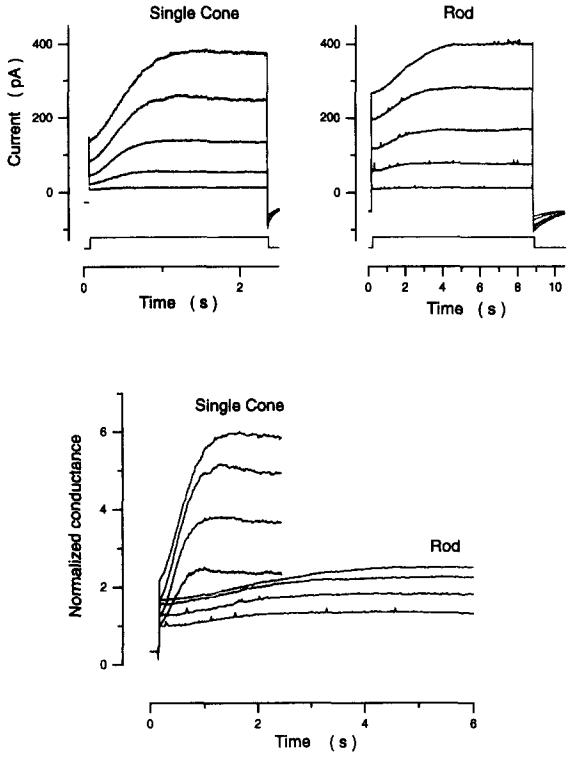

FIGURE 8. Comparison of DVAC in rods and cones. The upper, left panel illustrates outer segment currents measured in the dark with suction electrodes on a single cone isolated from the striped bass retina. Membrane voltage was controlled with a tight-seal electrode attached to the inner segment (Miller and Korenbrot, 1993*b*). Membrane voltage was held at −40 mV and currents were activated by 2.3-s voltage steps between +20 and +60 mV, in 10-mV increments, presented at 5-s intervals. The top right shows outer segment currents measured in the dark with perforated-patch electrodes in a whole rod isolated from tiger salamander. Membrane voltage was held at −30 mV and currents were activated by 8.65-s voltage steps between +20 and +60 mV, in 10-mV increments, presented at 20-s intervals. In the bottom, the same data is reploted on a common time axis and normalized by defining the initial conductance at +20 mV in both rods and cones to be unity.

Table II demonstrate that, at any voltage, the conductance enhancement in rods was slower and smaller than in cones. The differences in DVAC, when analyzed with the model presented in the next section, yield insights that may begin to explain the well-known differences in phototransduction signals between rods and cones.

THEORY

We have previously proposed a detailed mechanism to explain the generation of DVAC in cone photoreceptors (Miller and Korenbrot, 1993*b*). We have applied the

same model to the analysis of DVAC and DVIC in rods, with two significant differences: (*a*) the Ca^{2+}-dependence of GC is that defined by recent publications and (*b*) the recently described cGMP binding to specific outer segment sites is explicitly considered. The original publication (Miller and Korenbrot, 1993*b*) contains detailed justification for the equations used and their derivation. Here we simply restate each of the sequential events called for in the model, the most relevant equations governing the features of each event and the values assigned to the independent parameters.

Voltage-dependent decrease in cytoplasmic Ca^{2+} concentration. The model assumes that depolarizing voltage steps reduce Ca^{2+} influx because the electromotive driving force decreases as membrane voltage approaches the equilibrium potential of Ca^{2+}. The voltage-dependent decrease in Ca^{2+} influx, in the face of sustained Ca^{2+} efflux via the $Na^+/Ca^{2+},K^+$ exchanger, leads to a lowering of cytoplasmic Ca^{2+} concentration. The method to calculate changes in cytoplasmic Ca^{2+} (Sneyd and Tranchina, 1989; Miller and Korenbrot, 1993*b*) makes explicit assumptions about the fraction of

TABLE II

Comparison of Quantitative Features of DVAC in Rods and Cones

	Rod tiger salamander*		Single cone striped bass‡	
V_m	Conductance enhancement	Activation time§	Conductance enhancement	Activation time
mV	g_{max}/g_{init}	*s*	g_{max}/g_{init}	*s*
+30	1.13 ± 0.08	1.38 ± 0.34‖	1.51 ± 0.15	0.359 ± 0.057
+40	1.17 ± 0.09	1.23 ± 0.37	2.00 ± 0.20	0.409 ± 0.064
+50	1.23 ± 0.09	1.35 ± 0.42	2.34 ± 0.27	0.492 ± 0.082
+60	1.28 ± 0.11	1.73 ± 0.78	2.27 ± 0.28	0.570 ± 0.105

*n = 10, averaged ±SD.

‡n = 9, averaged ±SD.

§Activation time is the time necessary to reach 63% of the maximum current.

‖At this voltage, activation in five rods was too small to measure.

the current through the cGMP-gated channels that is carried by Ca^{2+}. Experimental estimates indicate that Ca^{2+} influx into outer segments is ~8–12% of the dark current in rods (Hodgkin, McNaughton, and Nunn, 1987; Nakatani and Yau, 1989; Lagnado et al., 1992), and ~15–25% in cones (Perry and McNaughton, 1991). In our computation, we assigned the Ca^{2+} influx to be 10 and 20% of the dark current in rods and cones, respectively.

Calculation of the voltage-dependent change in cytoplasmic Ca^{2+} concentration requires assignment of values to three unknown, adjustable parameters: γ_V, Ω^{-1} and τ_{exch}. γ_V is the ratio of the Ca^{2+} specific conductance of the cGMP channels at the command voltage ($g_{V_{comm}}$) over that at the holding voltage ($g_{V_{hold}}$). Ω^{-1}, as used before (Tranchina et al., 1991; Miller and Korenbrot 1993*b*), is the Ca^{2+} buffering power of the outer segment cytoplasm defined as the ratio of free Ca^{2+} ($[Ca^{2+}]_i$) over total Ca^{2+} ($[Ca^{2+}]_T$). τ_{exch} is the time constant of Ca^{2+} clearance from outer segment

due to the transport activity of the $Na^+/Ca^{2+},K^+$ exchanger. Thus,

$$\gamma_V = \frac{g_{V_{comm}}}{g_{V_{hold}}} \qquad \Omega^{-1} = \frac{[Ca]_i}{[Ca]_T}.$$

We selected values for the adjustable parameters by trial and error with the objective of minimizing the difference between simulated and experimental data. Although we had no constraint on the possible values of γ_V and Ω^{-1}, the value of τ_{exch} was initially selected to be near the time constant estimated from measurements of the electrogenic activity of the $Na^+/Ca^{2+},K^+$ exchanger; 90 ms for bass cones (Miller and Korenbrot, 1993*b*) and 600 ms for tiger salamander rods (Cobbs and Pugh, 1987; Lagnado et al., 1992).

Ca^{2+}-dependent activity of guanylyl cyclase. The most recent measurements in rods indicate the following equation governs the velocity of GC activity and its dependence on Ca^{2+}, $\{V_{GC}([Ca]_i)\}$:

$$V_{GC}([Ca]_i) = V_{GC}^{max} * \frac{[GTP]}{K_m + [GTP]} * \frac{\left(\frac{1}{[Ca]_i(V,t)}\right)^{2.2}}{\left(\frac{1}{K_d}\right)^{2.2} + \left(\frac{1}{[Ca]_i(V,t)}\right)^{2.2}} + V_{GC}^{*} \qquad (3)$$

where V_{GC}^{*} is the Ca^{2+}-independent activity of ~4 μM/s, V_{GC}^{max} is the maximum possible enzyme velocity of ~95 μM/s and K_d is the dissociation constant of Ca^{2+} with the enzyme with a value of 200 nM (Koch and Stryer, 1988; Koch, Eckstein, and Stryer, 1990; Lambrecht and Koch, 1991; personal communications from K. Palczewski and from A. Dizhoor and J. Hurley). In the simulations, guanylyl cyclase activity changes only with cytoplasmic Ca^{2+} concentration because we expect GTP concentration to remain constant at 1 mM, the concentration in the electrode-filling solution. We assumed the same equation describes the activity of guanylyl cyclase in rods and in cones.

Time-dependent change in cytoplasmic cGMP concentration. The time course of the change in cGMP concentration is the solution of the following differential equation:

$$\frac{d[cGMP]_T(t)}{dt} = V_{GC} - k_{d,\,PDE} * [cGMP]_f(t) \qquad (4)$$

where $[cGMP]_T(t)$ is the total cGMP concentration, V_{GC} is given by Eq. 3 and the second term in the equation computes the velocity of PDE (V_{PDE}). $k_{d,PDE}$ is the pseudo first-order rate constant of PDE in the dark and $[cGMP]_f(t)$ is the cytoplasmic concentration of free cGMP. We calculate V_{PDE} under the simplification that enzyme activity is of first-order because the standing concentration of free cGMP in the dark (4.7 μM in rods and 12.8 μM in cones, see below) is below the values reported for the K_m for cGMP of PDE in rods and cones, ~100 μM (review in Pugh and Lamb, 1993; Gillespie, 1990).

cGMP binding to specific outer segment sites. Eq. 4 computes the total cGMP generated by the coupled enzymatic system. Cote and Brunnock (1993) have recently identified two cGMP binding sites in rod outer segments (data from frog outer segments): one with dissociation constant K_a = 0.076 μM and a site density, $[S_a]$, of

30 μM and a second with dissociation constant K_b = 6.6 μM and a site density, $[S_b]$, of 78 μM. Binding of cGMP to the high affinity site, Sa, is slow, 50% with $t_{1/2}$ = 45 s and 44% with $t_{1/2}$ = 3.6 min. Because the time course of binding to the high affinity site is very slow when compared with the time course of DVAC and because at the physiological level of cGMP in the dark (in micromolar) these sites are saturated, we neglected the high affinity sites when calculating changes in free cGMP. We assumed that binding kinetics of the intermediate affinity sites, S_b, were rapid when compared with the rate of DVAC and, therefore, that these sites were at equilibrium at all times. Chemical equilibrium under these conditions indicates that:

$$K_b = \frac{[\text{cGMP}]_f * [S_b]}{[\text{cGMP}\cdot S_b]} \tag{5}$$

where $[\text{cGMP}]_f$ is the free cytoplasmic cGMP, $[S_b]$ is the concentration of free binding sites and $[\text{cGMP}\cdot S_b]$ is the concentration of complexed sites. Also,

$$[\text{cGMP}]_T = [\text{cGMP}]_f + [\text{cGMP}\cdot S_a] + [\text{cGMP}\cdot S_b]$$

and

$$[S]_T = [S]_f + [\text{cGMP}\cdot S_a] + [\text{cGMP}\cdot S_b]$$

where $[S]_T$ is the total concentration of binding sites. We used these equations to compute the change in free cGMP concentration (Segel, 1975), given the changes in total cGMP calculated through Eq. 4. We used the same values for K_a, K_b and $[S]_T$ to simulate data in cones. The calculated total cGMP concentration in the dark, that is, the sum of cGMP bound to high and low affinity sites plus the free cGMP was 61.9 μM in rods and 94.2 μM in cones.

Activation of membrane conductance by cGMP. The dependence of membrane conductance on cGMP concentration is given by:

$$\frac{g(t)}{g_{max}} = \frac{([\text{cGMP}]_f(t))^n}{K^n_{1/2} + ([\text{cGMP}]_f(t))^n} \tag{6}$$

where $g(t)$ is membrane conductance, g_{max} is the maximum value of this conductance, $[\text{cGMP}]_f(t)$ is the free cytoplasmic concentration of cGMP and $K_{1/2}$ is the binding constant of the ion channel for cGMP. In tiger salamander rods at +50 mV $K_{1/2}$ = 10 μM and n = 3 (Karpen et al., 1988). In bass single cones at +80 mV $K_{1/2}$ = 42 μM and n = 2.5 (Picones and Korenbrot, 1992).

The dark current amplitude is no more than 5% of the amplitude elicited by saturating levels of cytoplasmic cGMP both in rods (Cobbs and Pugh, 1985; Hestrin and Korenbrot, 1987) and cones (Cobbs, Barkdoll, and Pugh, 1985). In a detailed study in tiger salamander rods, Cameron and Pugh (1990) calculated that the outer segment current in the dark could be as little as 1.5% of the cGMP-saturated current. In our simulations we assigned $g(t)/g_{max}$ a value of 5% in darkness in both receptor types. Given this assignment, Eq. 6 indicates that the cytoplasmic concentration of free cGMP in darkness is 3.74 μM in rods and 12.8 μM in cones.

Simulation of DVAC in Intact Rods

To start the simulations, we assigned the free Ca^{2+} concentration in darkness a value of 270 nM in both rods and cones, based on experimental observations (Ratto et al., 1988; Korenbrot and Miller, 1989; Miller and Korenbrot, 1993*b*). At this cytoplasmic free Ca^{2+} concentration, Eq. 4 indicates that the guanylyl cyclase activity should be 20.18 μM/s. To be in steady state, therefore, PDE activity must also be 20.18 μM/s. Because the concentration of cGMP is 3.74 μM in rods and 12.8 μM in cones, then the first order rate constant of PDE, $k_{d,PDE}$, is 5.395 s^{-1} in rods and 1.576 s^{-1} in cones.

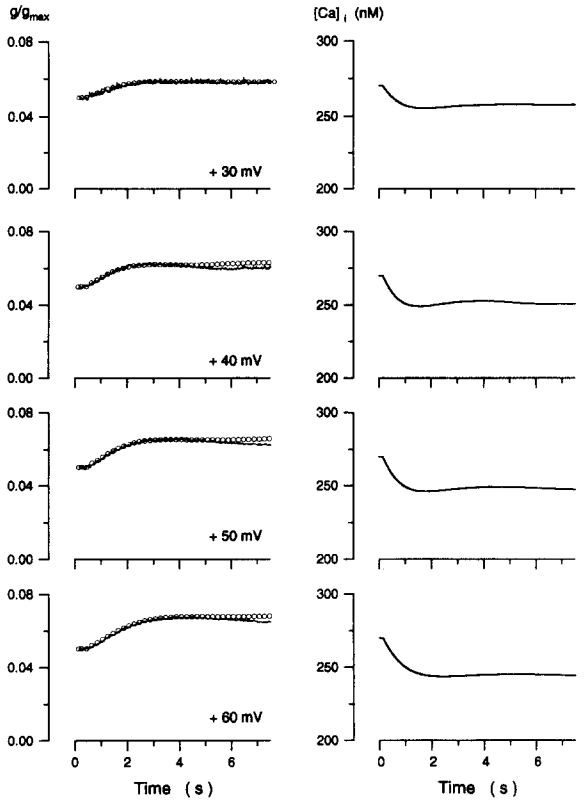

FIGURE 9. Fit of simulated data to DVAC measured in rods. The left illustrates, as a continuous line, the membrane conductance measured in the dark in response to depolarizing steps from a holding voltage of −30 mV to +30, +40, +50, or +60 mV, as labeled. The open circles in the left panels present the outer segment conductance simulated by the model that best fit the experimental data. The panels on the right illustrate the simulated changes in cytoplasmic Ca^{2+} concentration that underlie DVAC. The average value of the adjustable parameters used to obtain fits such as those shown are presented in Table III. The fits shown are typical of our data (squared difference between simulated and experimental data $\leq 10^{-4}$).

The time course and magnitude of conductance changes generated with the theoretical model simulated experimental data well. Fig. 9 illustrates experimental data measured in rods with the perforated-patch technique at depolarizing voltages between +30 and +60 mV; superimposed on the experimental data are simulated data. Also illustrated are the computed changes in cytoplasmic Ca^{2+} that underlie the simulated data. For the data shown, the sum of the squared differences between experimental and simulated values was $\leq 0.2 \times 10^{-4}$. Optimum matches of similar quality (squared difference between experimental and simulated data $\leq 10^{-4}$) between simulated and experimental data for nine rods yielded the average values of

the adjustable parameters listed in Table III. The estimated values of τ_{exch} were voltage dependent, and slowed down as the membrane depolarized. This voltage dependence is characteristic of the ion transport through the Na^+/Ca^{2+} exchanger in other cells as well (Lagnado and McNaughton, 1990).

Simulation of DVAC in Cones

In cones, data simulated with the theoretical model also fit experimental data well. Fig. 10 illustrates simulated data superimposed on experimental data measured in single cones of the striped bass (Miller and Korenbrot, 1993*b*). We also illustrate the computed changes in cytoplasmic Ca^{2+} that underlie the simulated data. The computed Ca^{2+} concentration at all voltages reached a minimum during the depolarization and then recovered to a steady state value. Optimum matches of similar quality (squared difference between experimental and simulated data $\leq 10^{-4}$)

TABLE III

Values of Parameters in Simulated DVAC

	Adjustable parameters			Computed parameters	
	τ_{exch}	Ω^{-1}	γ_v	$[Ca^{2+}]_i$ steady	$[Ca^{2+}]_i$ minimum
Rods*	*ms*			*nM*	*nM*
+30 mV	720 ± 115	0.0035 ± 0.0025	1.23 ± 0.23	257 ± 7	254 ± 8
+40 mV	644 ± 229	0.0035 ± 0.0030	1.37 ± 0.24	257 ± 9	254 ± 11
+50 mV	688 ± 214	0.0029 ± 0.0015	1.39 ± 0.17	253 ± 7	251 ± 8
+60 mV	772 ± 322	0.0024 ± 0.0016	1.36 ± 0.21	249 ± 8	248 ± 10
Single cones‡					
+30 mV	112 ± 16	0.0118 ± 0.0052	0.91 ± 0.16	216 ± 12	141 ± 26
+40 mV	130 ± 19	0.0101 ± 0.0034	0.73 ± 0.11	191 ± 11	106 ± 17
+50 mV	136 ± 16	0.0087 ± 0.0028	0.72 ± 0.08	180 ± 10	106 ± 18
+60 mV	142 ± 26	0.0069 ± 0.0025	0.79 ± 0.12	177 ± 9	115 ± 27

*n = 9, averages ±SD, except at +30 mV where n = 5 because in four rods activation was too small to measure.

‡n = 7, averages ±SD.

$\Omega^{-1} = [Ca]_i/[Ca]_T$.

$\gamma_v = g_{v_{comm}}/g_{v_{hold}}$.

between simulated and experimental data for seven single cones yielded the average values of the adjustable parameters listed in Table III.

Although the same theoretical model can explain DVAC in both rods and cones, the values of the adjustable parameters for each receptor type listed in Table III are very different. These quantitative differences in Ca^{2+} homeostasis revealed by DVAC must contribute significantly to the functional difference between rods and cones, given the critical role of Ca^{2+} in regulating the gain and time course of the photoresponse. The differences in Ca^{2+} homeostasis reflect differences in outer segment volume, Ca^{2+} clearance rates, Ca^{2+} buffering and the fraction of the current carried by Ca^{2+} through the cGMP-gated channels.

Simulation of DVIC in Rods Loaded with High Cytoplasmic Na^+

Since the outer segment conductance tracks cytoplasmic cGMP concentration, DVIC observed in Na^+-loaded rods likely reflects a voltage-dependent lowering of free cGMP concentration. DVIC, therefore, can arise from GC inactivation, as might occur if depolarization raises rather than lowers cytoplasmic Ca^{2+} level in the dark. The model developed above to explain DVAC can also explain DVIC in rods if one additional adjustment is allowed. If the cytoplasmic free Ca^{2+} concentration in darkness at the holding potential is not constrained to an initial value of 270 nM, as

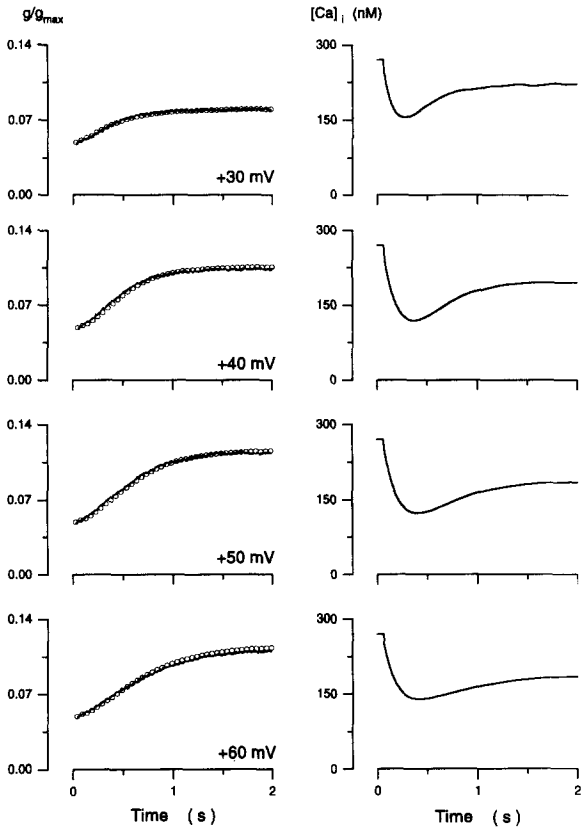

FIGURE 10. Fit of simulated data to DVAC measured in single cones. The left illustrates, as a continuous line, the membrane conductance measured in the dark in response to depolarizing steps from a holding voltage of −40 mV to +30, +40, +50, or +60 mV, as labeled. The open circles in the left present the outer segment conductance simulated by the model that best fit the experimental data. The right illustrates the simulated changes in cytoplasmic Ca^{2+} concentration that underlie DVAC. The average value of the adjustable parameters used to obtain fits such as those shown are presented in Table III. The fits shown are typical of our data (squared difference between simulated and experimental data $\leq 4 \times 10^{-4}$).

discussed for DVAC, but is allowed to take higher values, then the kinetic model can generate DVIC-like signals that can be made to fit experimental results. The reduction in transport activity of the $Na^+/Ca^{2+},K^+$ exchanger expected in the outer segment of Na-loaded rods, will almost certainly result in higher cytoplasmic Ca^{2+} concentration when compared with that of normal cells. Also, rods loaded with Hi Na-TSIS have a positive holding current at −30 mV and a smaller saturated photocurrent amplitude when compared with intact rods (see above). This electrical behavior is characteristic of rods with elevated intracellular Ca^{2+} (Lamb and Matthews, 1988).

Fig. 11 illustrates an example of experimental DVIC conductances fit with simulations generated by the kinetic model under the assumption that the dark cytoplasmic Ca^{2+} at holding voltage was 750 nM. Also shown are the simulated Ca^{2+} concentration changes that are presumed to underlie the conductance inactivation. In these simulations, Ca^{2+} concentration at all voltages is seen to rise to an initial peak and then decline back towards the starting value. It is this rise in Ca^{2+} concentration that quenches the dark GC activity. Because GC and PDE are active in darkness, this results in the net loss of free cGMP. The simulation suggests that Ca^{2+} rises with depolarization, despite the decrease in electromotive force because the

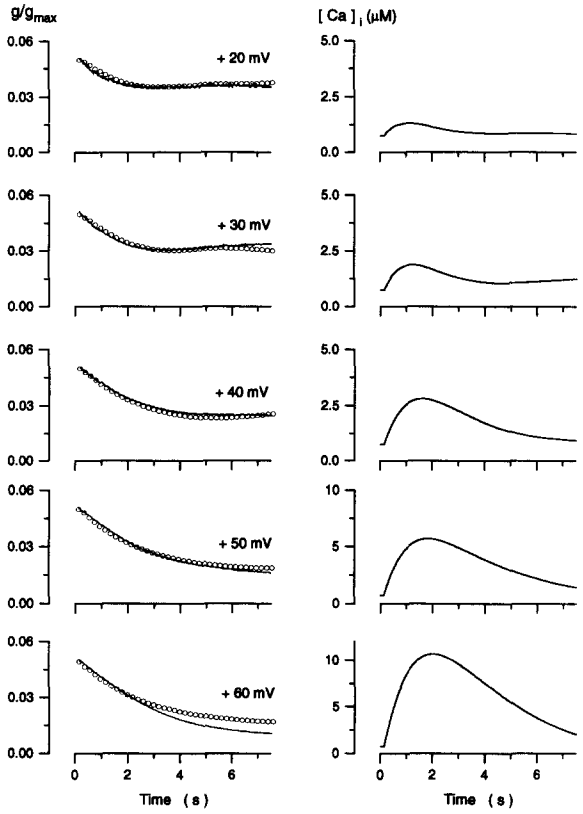

FIGURE 11. Fit of simulated data to DVIC measured in rods. Panels on the left illustrate as a continuous line the membrane conductance measured in the dark in response to depolarizing steps from a holding voltage of −30 mV to +30, +40, +50, or +60 mV, as labeled. The open circles in the left present the outer segment conductance simulated by the model that best fit the experimental data. The panels on the right illustrate the simulated changes in cytoplasmic Ca^{2+} concentration that underlie DVIC. The fits shown are typical of our data.

Ca^{2+}-specific conductance of the cGMP-gated channels increases greatly as the voltage depolarizes. For example, the simulated data shown in Fig. 11 were generated with values of γ_V = 3.5 at +30 mV, 5 at +40 mV, 10 at +50 mV, and 19 at +60 mV. The average value of Ω^{-1} at all voltages was 0.5 (compare with data in Table III). After reaching peak, Ca^{2+} declines simply because the channels are closing as the cGMP concentration declines. We succeeded in matching simulated and experimental DVIC data in every cell we tried (n = 4). In all cases, however, the model fails to fit data generated by large depolarizations (Fig. 11). The failure at high voltages is likely to arise from our neglect of the high affinity cGMP binding sites,

sites that will become functionally important as the cGMP concentration decreases to very low values, as it must when the outer segment current is small. We did not explore extensively the statistics of the successful DVIC model. However, in the four simulations investigated, we found the range of initial Ca^{2+} concentrations was from 550 to 750 nM, and the range of peak Ca^{2+} concentrations at, for example, +40 mV was from 2.85 to 28 μM.

DISCUSSION

In both rods and cones, membrane depolarization in darkness activates outer segment-specific currents we have termed DVAC. We have previously described the features of DVAC in cones (Miller and Korenbrot, 1993*b*). Rispoli and Detwiler (1991) first recognized DVAC in detached rod outer segments of gecko. Although Baylor and Nunn (1986) first explored the effects of depolarization on rod outer segment currents in the dark, they reported observing voltage-inactivated currents, which we have termed DVIC, rather than DVAC. The results presented here indicate that DVIC occurs in rods whose cytoplasm has an abnormal ionic composition. Elevated intracellular Na^+ (39 mM) is associated with robust DVIC (Fig. 6), while elevated Ca^{2+} is associated with a weak DVIC (Fig. 5). The DVIC observed by Baylor and Nunn (1986) likely reflects abnormal cytoplasmic accumulation of Na^+ and/or Ca^{2+} under their experimental conditions. Examination of their published records reveals that some rods in their hands did display DVAC (see their Fig. 5). Intact rods with unperturbed cytoplasm, best represented in our results by data measured with the perforated-patch methods, only display DVAC.

DVAC with characteristics similar to those of intact rods can be measured with conventional tight-seal electrodes, either in whole rods or in detached rod outer segments, provided the composition of the electrode-filling is carefully controlled. We found that control of Ca^{2+} and Na^+ concentrations and removal of multivalent cations with Chelex-100 was essential to observe DVAC with conventional whole-cell recordings. It is noteworthy that the use of Chelex-100 was not necessary to record DVAC in cones with tight-seal electrodes. This suggests that cones are more effective than rods in maintaining their normal ionic composition, in particular the concentration of free Ca^{2+}, in the face of an experimental challenge. It is intriguing that cones loaded with intracellular Na^+ at the same concentration that sustains DVIC in rods did not demonstrate photocurrents at all (unpublished observation). Indeed, DVIC-like behavior was never observed in cones under any of the various conditions that generate DVIC in rods. Differences between rods and cones in the regulation of Ca^{2+} homeostasis by cytoplasmic Na^+ may be functionally important under conditions that change cytoplasmic Na^+ concentration, for example, prolonged exposure to bright light. This feature may merit future exploration.

Voltage-dependent Changes in Cytoplasmic Ca^{2+}

We calculated the time course and magnitude of voltage-dependent changes in cytoplasmic Ca^{2+} in the outer segment with a model that makes explicit choices about the voltage dependence of the Ca^{2+}-specific conductance of the cGMP-gated channels, the Ca^{2+} buffering in the cytoplasm and the time constant of clearance of Ca^{2+}

from the outer segment. The model, however, does not consider possible diffusional delays between Ca^{2+} concentration changes near the membrane, where the transporters are located, and the site where guanylyl cyclase is located. This is acceptable because the time constant of development of DVAC is slow when compared with diffusion limited transit times of Ca^{2+}. In outer segments of rods and cones, Ca^{2+} concentration can be expected to equilibrate within ~100 ms, if limited by aqueous diffusion.

Cytoplasmic Ca^{2+} buffering power has been experimentally studied only in tiger salamander rods (Lagnado et al., 1992). The estimates of Ca^{2+} buffering we obtained by model fitting are in excellent agreement with those measured by Lagnado et al. (1992). However, their experimental measurements recognize the existence of two Ca^{2+} binding sites, whereas we have simply modeled a single one. Ca^{2+} buffering in cones has not been measured directly, but we predict it to be ~fourfold less effective than that in rods. A striking prediction of the model fitting is a weak voltage-dependence for the Ca^{2+} buffering power in cones, but not in rods (Table III). We speculate that the predicted higher Ca^{2+} buffer in rods may be related to the presence of discs, known to bind and retain high Ca^{2+} concentrations against a concentration gradient (Fain and Schroeder, 1990). In cones, the voltage dependence of Ca^{2+} buffering may reflect the buffering role of unstirred layers on the membrane surface, layers that may be affected by changes in the transmembrane voltage (McLaughlin and Brown, 1981), including those generated during the photoresponse.

Activity and Ca^{2+} Dependence of the Enzymes of Transduction in Rods and Cones

All the biochemical processes invoked to explain DVAC have been characterized in rods, generally bovine rods. Much less is known about the corresponding biochemical events in cones. Where it has been possible to test, the functional properties of the enzymes of transduction in cones appear similar to those of rods (Hestrin and Korenbrot, 1990; Miller et al., 1994). DVAC signals are remarkably different in rods and cones. Yet, we succeeded in simulating DVAC in both rods and cones with the explicit assumption that the biochemical events underlying DVAC, namely, the activity of GC, its Ca^{2+} dependence and the binding of cGMP to specific sites are identical in the two receptor types. This success suggests that the differences in the transduction signal between rods and cones arise from differences in the gain and the kinetics of the light-dependent changes in cytoplasmic Ca^{2+}, rather than from differences in the Ca^{2+} regulation of the activity of the enzymes of transduction. While differences in Ca^{2+} homeostasis and in the speed and magnitude of Ca^{2+} concentration changes must be important, we do not hold that they alone are sufficient to fully account for the differences in transduction between rods and cones. Experimental evidence demonstrates that preventing light-dependent changes in Ca^{2+} concentration does not trivially convert the photocurrent of a cone into one like that of a rod (Nakatani and Yau, 1989; Matthews et al., 1990; Miller and Korenbrot, 1993*b*).

Rates of Ca^{2+} Clearance from the Outer Segment

The quantitative differences in Ca^{2+} homeostasis between rods and cones reflect differences in the outer segment volume, in addition to the Ca^{2+} flux through the cGMP-gated channels, the intracellular Ca^{2+} buffering capacity and the rate of Ca^{2+} clearance. Volume is important because the conversion of a given Ca^{2+} flux rate into a concentration change depends directly on this parameter (Sneyd and Tranchina, 1989; Miller and Korenbrot, 1993*b*). Through our simulations, we determined that every one of the four parameters cited above is important in determining the difference in Ca^{2+} homeostasis between rods and cones. Computer exploration demonstrated that keeping a given parameter invariant, any one, while allowing the other three to vary was never sufficient to successfully simulate DVAC in both rods and cones.

Differences in the outer segment Ca^{2+} clearance rate between rods and cones have been previously recognized from measurements of the electrogenic transport through the $Na^+/Ca^{2+},K^+$ exchanger (Hestrin and Korenbrot, 1990). The differences between rods and cones may arise in part from the difference in surface to volume ratio of their respective outer segments: at a constant volume, cone outer segments have a larger surface than that of the rod's because of multiple infolding of the plasma membrane. It is interesting to note, for example, that cones in tiger salamander and striped bass have rather different size and volume (tiger salamander $4.5 \times 8.5 \times 3$ μm, base diameter × height × tip diameter, volume 95 μm^3, striped bass $5 \times 15 \times 3$ μm, volume 192 μm^3), yet their surface to volume ratio, calculated assuming a 300-Å repeat distance between discs, is essentially the same, 65. The electrically determined time constant of Ca^{2+} clearance in tiger salamander cones is ~90 ms (Hestrin and Korenbrot, 1990), and it is ~110 ms in striped bass cones (Miller and Korenbrot, 1993*b*). Surface to volume ratios alone, however, do not predict the differences in Ca^{2+} clearance rates between rods and cones. In tiger salamander rods, the surface to volume ratio is 0.36, compared with 65 for cones, yet the Ca^{2+} clearance rate in rod outer segments is only six- to eightfold slower than that in cones. The membrane density and/or the intrinsic transport rates of the $Na^+/Ca^{2+},K^+$ transporters, therefore, must be different in rods and cones.

cGMP-gated Channels in Rods and Cones

Differences in the ion permeation properties of the cGMP-gated channels of rods and cones are important contributors to the functional difference between the two receptor types. The fraction of the dark current carried by Ca^{2+} is higher in cones than in rods (Perry and McNauhton, 1991) and this is an explicit assumption in our simulations. Permeability measurements under biionic conditions in detached outer segment membrane patches suggest that P_{Ca}/P_{Na} is larger in cones (Haynes, 1993) than rods (Zimmerman and Baylor, 1992; Karpen, Brown, Stryer, and Baylor, 1993). However, the precise values for P_{Ca}/P_{Na} for rod or cone outer segment membranes under ionic gradients similar to those in intact cells are unknown. Differences in the characteristics of the interaction of cations with the cGMP-gated channels of rods and cones are now recognized (reviewed in Picones and Korenbrot, 1992). The results presented here, again, reflect differences between rods and cones in the interaction

of cations with the cGMP-dependent channels: 39 mM cytoplasmic Na^+ generates DVIC in rods, but not in cones. Our simulations suggest that DVIC arises from Na^+-dependent changes in the interaction of Ca^{2+} with the cGMP-gated channels, such that in high cytoplasmic Na^+, at depolarized voltages, the Ca^{2+} flux through the channels is much larger than in the low Na^+ of the unpurturbed rod. In cones, in contrast, elevated cytoplasmic Na^+ blocked the photocurrent. If the Ca^{2+} conductance of the channel in cones is higher than in rods, as we have suggested above, and Na^+ enhances this even further, then the photocurrent blocking effect of Na^+ in cones is likely to reflect excessive loading of cytoplasmic Ca^{2+} in the outer segment.

Conclusion

Our interest in exploring the biochemical and biophysical basis for DVAC is based on the presumption that the differences in Ca^{2+} homeostasis between rods and cones revealed by DVAC in the dark also operate when light, rather than voltage, cause changes in cytoplasmic free Ca^{2+}. Depolarizing voltage reduces Ca^{2+} influx by reducing the electromotive driving force, whereas light does it by reducing membrane conductance. Our data on DVAC indicate that a given reduction in Ca^{2+} influx through the cGMP-gated channels, whether caused by light or by depolarization, will cause a decrease in free Ca^{2+} concentration that is larger and faster in cones than in rods. Guanylyl cyclase is a Ca^{2+}-regulated enzyme that may be functionally identical in rods and cones. If, for a given change in photocurrent, changes in free Ca^{2+} are larger and faster in cones than in rods, then the activation of GC should be faster and more robust in cones than in rods. Because activation of guanylyl cyclase effectively opposes the action of the light-activated PDE, then the light-dependent changes in cGMP concentration should be smaller and faster in cones than in rods. This could explain the faster time course and decreased sensitivity of the cone photocurrent when compared with that of the rod. Other Ca^{2+}-dependent processes (Kawamura, 1993; Kawamura et al., 1993; Lagnado and Baylor, 1994) can also be expected to exhibit faster kinetics and larger magnitudes in cones than in rods. Direct measurements of the light- and voltage-dependent changes in outer segment Ca^{2+} concentration must be obtained to confirm our thesis.

We are grateful to D. Hackos, D. Julian, A. Olson, A. Picones, and T. Rebrik for their thoughtful review of our manuscript. We thank P. Detwiler for sharing his unpublished observation that detached rod outer segments from Gecko exhibit DVIC in the presence of high cytoplasmic Na.

Original version received 17 February 1994 and accepted version received 20 June 1994.

REFERENCES

Babashak, J. V., and T. M. Phillips. 1989. Isolation of a specific membrane protein by immunoaffinity chromatography with biotinylated antibodies immobilized on avidin coated glass beads. *Journal of Chromatography.* 476:187–194.

Bader, C. R., D. Bertrand, and E. A. Schwartz. 1982. Voltage-activated and Ca^{2+}-activated currents studied in solitary rod inner segments from the salamander retina. *Journal of Physiology.* 331:253–284.

Baylor, D. A., and T. D. Lamb. 1982. Local effects of bleaching in retinal rods of the toad. *Journal of Physiology.* 328:49–71.

Baylor, D. A., and B. J. Nunn. 1986. Electrical properties of the light-sensitive conductance of rods of the salamander *Ambystoma tigrinum*. *Journal of Physiology*. 371:115–145.

Cameron, D. A., and E. N. Pugh, Jr. 1990. The magnitude, time course and spatial distribution of current induced in salamander rods by cyclic guanine nucleotides. *Journal of Physiology*. 430:419–439.

Cobbs, W. H., A. E. Barkdoll III, and E. N. Pugh, Jr. 1985. Cyclic GMP increases photocurrent and light sensitivity of retinal cones. *Nature*. 317:64–66.

Cobbs, W. H., and E. N. Pugh, Jr. 1985. Cyclic GMP can increase rod outer segment light sensitive current 10-fold without delay of excitation. *Nature*. 313:585–587.

Cobbs, W. H., and E. N. Pugh, Jr. 1987. Kinetics and components of the flash photocurrent of isolated retinal rods of the larval salamander, *Ambystoma tigrinum*. *Journal of Physiology*. 394:529–572.

Corey, D. P., J. M. Dubinsky, and E. A. Schwartz. 1984. The Ca current in inner segments of rods from salamander (*Ambystoma tigrinum*) retina. *Journal of Physiology*. 254:557–575.

Cote, R. H., and M. A. Brunnock. 1993. Intracellular cGMP concentration in rod photoreceptors is regulated by binding to high and moderate affinity cGMP binding sites. *Journal of Biological Chemistry*. 268:17190–17198.

Fain, G. L., T. D. Lamb, H. R. Matthews, and R. L. W. Murphy. 1989. Cytoplasmic calcium as the messenger for light-adaptation in salamander rods. *Journal of Physiology*. 416:215–243.

Fain, G. L., and W. H. Schroeder. 1990. Light-induced Ca release and re-uptake in toad rods. *Journal of Neuroscience*. 10:2238–2249.

Fleischman, D., and M. Denisevich. 1979. Guanylate cyclase of isolated bovine retinal rods. *Biochemistry*. 18:5060–5066.

Gillespie, P. G. 1990. Phosphodiesterases in visual transduction by rods and cones. *In* Cyclic Nucleotide Phosphodiesterases: Structure, Regulation and Drug Action. J. Beavo and M. D. Houslay, editors. Wiley Interscience, NY.

Hagins, W. A., R. D. Penn, and S. Yoshikami. 1970. Dark current and photocurrent in retinal rods. *Biophysical Journal*. 10:380–412.

Haynes, L. W. 1993. Mono- and divalent cation selectivity of catfish cone outer segment cGMP-gated channels. *Biophysical Journal*. 64:A133. (Abstr.)

Haynes, L. W., A. R. Kay, and K. W. Yau. 1986. Single cGMP-activated channel activity in excised patches of rod outer segment membranes. *Nature*. 321:66–70.

Hestrin, S., and J. I. Korenbrot. 1990. Activation kinetics of retinal cones and rods: response to intense flashes of light. *Journal of Neuroscience*. 10:1967–1973.

Hestrin, S., and J. I. Korenbrot. 1987. Effects of cyclic GMP on the kinetics of the photocurrent in rods and in detached rod outer segments. *Journal of General Physiology*. 90:527–551.

Hodgkin, A. L., P. A. McNaugton, and B. J. Nunn. 1987. Measurement of sodium calcium exchange in salamander rods. *Journal of Physiology*. 391:347–370.

Horn, R., and A. Marty. 1988. Muscarinic activation of ionic currents measured by a new whole-cell recording method. *Journal of General Physiology*. 92:145–159.

Hsu, Y.-T., and R. S. Molday. 1993. Modulation of the cGMP-gated channel of rod photoreceptor cells by calmodulin. *Nature*. 361:76–79.

Hurley, J. B. 1992. Signal transduction enzymes of vertebrate photoreceptors. *Journal of Bioenergetics and Biomembranes*. 24:219–226.

Karpen, J. W., R. L. Brown, L. Stryer, and D. A. Baylor. 1993. Interaction between divalent cations and the gating machinery of cyclic GMP-activated channels in salamander retinal rods. *Journal of General Physiology*. 101:1–25.

Karpen, J. W., A. L. Zimmerman, L. Stryer, and D. A. Baylor. 1988. Gating kinetics of the cyclic GMP-activated channel of retinal rods: flash photolysis and voltage-jump studies. *Proceedings of the National Academy of Sciences, USA.* 85:1287–1291.

Kaupp, U. B., and K.-W. Koch. 1992. Role of cGMP and Ca in vertebrate photoreceptor excitation and adaptation. *Annual Review of Physiology.* 54:153–175.

Kawamura, S. 1993. Rhodopsin phosphorylation as a mechanism of regulation of cyclic GMP phosphodiesterase by S-modulin. *Nature.* 362:855–857.

Kawamura, S., and M. Murakami. 1991. Calcium-dependent regulation of cyclic GMP phosphodiesterase by a protein from frog retinal rods. *Nature.* 349:420–423.

Kawamura, S., and M. Murakami. 1989. Regulation of cGMP levels by guanylate cyclase in truncated frog rod outer segments. *Journal of General Physiology.* 94:649–668.

Koch, K-W., F. Eckstein, and L. Stryer. 1990. Stereochemical course of the reaction catalyzed by guanylate cyclase from bovine retinal rod outer segments. *Journal of Biological Chemistry.* 265:9659–9663.

Koch, K-W., and L. Stryer. 1988. Highly cooperative feed-back control of retinal rod guanylate cyclase by calcium ion. *Nature.* 334:64–66.

Korenbrot, J. I., and D. L. Miller. 1986. Calcium ions act as modulators of intracellular information flow in retinal rod phototransduction. *Neuroscience Research.* 4:S11–S34.

Korenbrot, J. I., and D. L. Miller. 1989. Cytoplasmic free calcium concentration in dark-adapted retinal rod outer segments. *Vision Research.* 29:939–948.

Lagnado, L., and D. A. Baylor. 1994. Calcium controls light-triggered formation of catalytically active rhodopsin. *Nature.* 367:173–277.

Lagnado, L., L. Cervetto, and P. A. McNaughton. 1992. Calcium homeostasis in the outer segments of retinal rods from the tiger salamander. *Journal of Physiology.* 455:111–142.

Lagnado, L., and P. A. McNaughton. 1990. Electrogenic properties of the Na:Ca exchange. *Journal of Membrane Biology.* 113:177–191.

Lamb, T. D., and H. R. Matthews. 1988. External and internal actions on the response of salamander retinal rods to altered external calcium concentration. *Journal of Physiology.* 403:473–494.

Lamb, T. D., H. R. Matthews, and V. Torre. 1986. Incorporation of calcium buffers into salamander retinal rods: a rejection of the calcium hypothesis of phototransduction. *Journal of Physiology.* 372:315–340.

Lambrecht, H.-G., and K.-W. Koch. 1991. A 26 kD calcium binding protein from bovine rod outer segment as modulator of photoreceptor guanylate cyclase. *EMBO Journal.* 10:793–798.

Lolley, R. N., and E. Racz. 1982. Calcium modulation of cyclic GMP synthesis in rat visual cells. *Vision Research.* 22:1481–1486.

Matthews, H. R. 1991. Incorporation of chelator into guinea-pig rod shows that Calcium mediates mammalian photoreceptor light adaptation. *Journal of Physiology.* 436:93–105.

Matthews, H. R., G. L. Fain, R. L. W. Murphy, and T. D. Lamb. 1990. Light adaptation in cones of the salamander: a role for cytoplasmic calcium concentration. *Journal of Physiology.* 420:447–469.

McLaughlin, S., and J. E. Brown. 1981. Diffusion of Ca ions in retinal rods. *Journal of General Physiology.* 77:475–483.

McNaughton, P. A. 1990. Light response of vertebrate photoreceptors. *Physiological Reviews.* 70:847–883.

McNaughton, P. A., L. Cervetto, and B. J. Nunn. 1986. Measurement of the intracellular free calcium concentration in salamander rods. *Nature.* 322:261–263.

Miller, D. L., and J. I. Korenbrot. 1987. Kinetics of light-dependent Ca fluxes across the plasma membrane of rod outer segments. A dynamic model of the regulation of cytoplasmic Ca concentration. *Journal of General Physiology.* 90:397–426.

Miller, J. L., and J. I. Korenbrot. 1993*a*. Phototransduction and adaptation in rods, single cones and twin cones of the striped bass retina: a comparative study. *Visual Neuroscience.* 10:653–667.

Miller, J. L., and J. I. Korenbrot. 1993*b*. In retinal cones, membrane depolarization in darkness activates the cGMP-dependent conductance: a model of Ca homeostasis and the regulation of guanylate cyclase. *Journal of General Physiology.* 101:933–961.

Miller, J. L., A. Picones, and J. I. Korenbrot. 1994. Differences in transduction between rod and cone photoreceptors: an exploration of the role of Ca homeostasis. *Current Opinion in Neurobiology.* 4:488–495.

Nakatani, K., and K.-W. Yau. 1988. Calcium and light adaptation in retinal rods and cones. *Nature.* 334:69–7X.

Nakatani, K., and K.-W. Yau. 1989. Calcium and magnesium fluxes across the plasma membrane of the toad rod outer segment. *Journal of Physiology.* 395:695–729.

Nakatani, K., and K.-W. Yau. 1989. Sodium-dependent calcium extrusion and sensitivity regulation in retinal cones of the salamander. *Journal of Physiology.* 409:525–549.

Pepe, I. M., A. Boero, L. Vergani, I. Panfoli, and C. Cugnoli. 1986. Effect of light and calcium on cyclic GMP synthesis in rod outer segments of toad retina. *Biochimica et Biophysica Acta.* 889:271–276.

Perry, R. J., and P. A. McNaughton. 1991. Response properties of cones from the retina of the tiger salamander. *Journal of Physiology.* 433:561–587.

Picones, A., and J. I. Korenbrot. 1992. Permeation and interaction of monovalent cations with the cGMP-gated channel of cone photoreceptors. *Journal of General Physiology.* 100:647–673.

Pugh, E. N., Jr., and T. D. Lamb. 1993. Amplification and kinetics of the activation steps in phototransduction. *Biochimica et Biophysica Acta.* 1141:111–149.

Rae, J., K. Cooper, P. Gates, and M. Watsky. 1991. Low access resistance perforated patch recordings using amphotericin B. *Journal of Neuroscience Methods.* 37:15–26.

Ratto, G. M., R. Payne, R. G. Owen, and R. Y. Tsien. 1988. The concentration of cytosolic free calcium in vertebrate rod outer segment measured with Fura-2. *Journal of Neuroscience.* 8:3240–3246.

Rispoli, G., and P. B. Detwiler. 1991. Voltage dependence of light-sensitive and Na/Ca exchange currents in detached lizard retinal rod outer segments. *Biophysical Journal.* 59:534*a*. (Abstr.)

Rispoli, G., W. A. Sather, and P. B. Detwiler. 1993. Visual transduction in dialyzed detached rod outer segments from lizard retina. *Journal of Physiology.* 465:513–537.

Sala, S., R. V. Parsey, A. S. Cohen, and D. R. Matteson. 1991. Analysis and use of the perforated patch technique for recording ionic currents in pancreatic B-cells. *Journal of Membrane Biology.* 122:177–187.

Segel, I. H. 1975. Biochemical calculations. John Wiley and Sons, Inc., NY.

Sneyd, J., and D. Tranchina. 1989. Phototransduction in cones: an inverse problem in enzyme kinetics. *Bulletin of Mathematical Biology.* 51:749–784.

Stryer, L. 1991. Visual excitation and recovery. *Journal of Biological Chemistry.* 266:10711–10714.

Tranchina, D., J. Sneyd, and I. D. Cadenas. 1991. Light-adaptation in turtle cones. Testing and analysis of a model for phototransduction. *Biophysical Journal.* 60:217–237.

Yau, K.-W., and D. A. Baylor. 1989. Cyclic GMP-activated conductance of retinal photoreceptor cells. *Annual Review of Neuroscience.* 12:289–327.

Yau, K.-W., and K. Nakatani. 1985. Light-induced reduction of cytoplasmic free calcium in retinal rod outer segment. *Nature.* 313:579–582.

Zimmerman, A. L., and D. A. Baylor. 1992. Cation interaction within the cyclic-GMP-activated channel of retinal rods from the tiger salamander. *Journal of Physiology.* 449:759–783.

Zimmerman, A. L., and D. A. Baylor. 1986. Single-channel currents from the cyclic GMP sensitive conductance of retinal rod outer segments. *Nature.* 321:70–72.